Original Paper

Sedimentological and geochemical characteristics of lower Cambrian Qiongzhusi shale in the Sichuan Basin and its periphery, SW China: Implications for differences in organic matter enrichment

Cheng-Lin Ye [a, b], Jun-Jun Shen [a, *], Shan-Shan Li [c], Yu-Man Wang [d], Guang-Chao Tan [c], Jia-Kai Yan [c], Lin Zhou [e], Ji-Yong Liu [e]

[a] Hubei Cooperative Innovation Center of Unconventional Oil and Gas of Yangtze University, Wuhan, 430100, Hubei, China
[b] College of Geophysics and Petroleum Resources, Yangtze University, Wuhan, 430100, Hubei, China
[c] Hydrogeology and Engineering Geology Institute of Hubei Geological Bureau, Jingzhou, 434020, Hubei, China
[d] PetroChina Research Institute of Petroleum Exploration and Development, Beijing, 100083, China
[e] Exploration and Production Research Institute, Jianghan Oilfield Company, SINOPEC, Wuhan, 430100, Hubei, China

A B S T R A C T

Few studies have systematically investigated the factors controlling organic matter enrichment in shales from the Qiongzhusi Formation, within and surrounding the Sichuan Basin, under different depositional environments. This has resulted in different academic understandings and limited clarity on the mechanisms of organic matter enrichment. On this premise, in this study, the basic geological characteristics and depositional paleoenvironments of shales along the passive continental margin, the western Hubei Trough, and the western Sichuan Trough were compared and analyzed using core, outcrop, and mineral testing. Furthermore, data from organic geochemical and elemental analyses were utilized to investigate the different enrichment mechanisms and formation modes of the organic matter in different periods. The results reveal that the organic matter enrichment in this region should be mainly influenced by the preservation conditions, paleo-productivity, and terrigenous input. However, there were clear differences in the main controlling factors in the different periods. In the Q1 phase, the region had a high sea level, had the strongest rifting, had the largest accommodation space, and exhibited characteristics of low terrestrial input and bottom water hypoxia. The changes in the paleo-productivity caused by upwelling currents were the main factors controlling the variations in the organic matter enrichment. In the Q2 phase, the weakened decreasing sea level co-occurred with a reduction in the accommodation space across the region. The organic matter enrichment was significantly controlled by the paleo-productivity, preservation conditions, and terrigenous inputs, and the organic matter enrichment conditions deteriorated from the passive continental margin to the western Hubei Trough and western Sichuan Trough. The total organic carbon (TOC) content of the shale decreased significantly. In the Q3 phase, the entire region entered an infilling stage, which was dominated by an oxygen-rich environment, and the preservation conditions were the decisive factor controlling the organic matter enrichment. The TOC content was low overall, and there were no evident differences across the different zones.

© 2024 The Authors. Publishing services by Elsevier B.V. on behalf of KeAi Communications Co. Ltd. This is an open access article under the CC BY-NC-ND license (http://creativecommons.org/licenses/by-nc-nd/4.0/).

1. Introduction

The Ediacaran-Cambrian (E-C) was one of the key transitional periods in geological history, during which a series of biological and geological events occurred. These included the breakup of the Rodinia supercontinent and the suturing of the Gondwana continent (Zhang et al., 2015a; Zhao et al., 2018), the global Sturtian and Marinoan glaciations and retreat (Hoffman and Li, 2009; Zhao and Zheng, 2011), the extinction of the Ediacaran fauna and the Cambrian explosion, and the evolution of the paleo-marine environment (Goldberg et al., 2007; Erwin et al., 2011; Laflamme et al., 2013; Chang et al., 2018; Liu et al., 2022a). Globally, a series of black

shale formations (Awan et al., 2020) were widely distributed at the base of the Early Cambrian in various regions including China, India, South Australia, Canada, southern France, and the UK. The tectonic evolution of the Yangtze Block during the Ediacaran to Early Cambrian transition period resulted in the formation of a passive continental margin basin with its southeastern portion giving rise to the South China Sea and its northwestern part forming the Qinling Sea. This basin was situated on Gondwana's northern margin (Li et al., 2008). The Sichuan Basin and its adjacent areas were situated on the northeastern margin of the Yangtze Craton, encompassing undisturbed sedimentary and continuous Precambrian-Cambrian strata (Fang et al., 2019; Wu et al., 2020a). Studies on the tectonic-sedimentological characteristics indicate that regional rifting of the Yangtze Plate began to peak in the Early Cambrian (Liu et al., 2016), which was accompanied by a large-scale global transgression (Wu et al., 2020a; Liu et al., 2022a). Black shale rich in organic matter was extensively deposited within the Qiongzhusi Formation in the Yangtze region, along with chert, phosphorite, barite, and polymetallic minerals such as minerals containing Ni, Mo, U, and V (Jin et al., 2016; Gao et al., 2018). Therefore, this region is a prime location for studying the relationships between the depositional paleoenvironment and organic matter enrichment.

Although predecessors have conducted numerous useful studies on the depositional environments and organic matter enrichment of the Qiongzhusi Formation in the Yangtze region, there are still significant theoretical differences regarding the main controls and formation mechanisms (Gu et al., 2022). Some scholars believe that the high paleo-productivity level in the Early Cambrian was the main factor controlling the organic matter enrichment (Xiang et al., 2018; Wang et al., 2019, 2020); while others have pointed out that there was clear ocean stratification in the Yangtze region during the Early Cambrian, resulting in anoxic-sulfide-ferruginous bottom water conditions, which controlled the enrichment of organic matter (Canfield et al., 2008; Chang et al., 2018; Xia et al., 2020; He et al., 2021). Several studies have reported that upwelling currents and hydrothermal activities provide abundant nutrients and favorable preservation conditions, which are conducive to organic matter enrichment (Xia et al., 2017; Yeasmin et al., 2017; Awan et al., 2020; Wu et al., 2020b; Liu et al., 2022a). Additionally, the paleoclimate, sea level rise, sedimentation rate, and terrigenous input have also been shown to influence the enrichment of organic matter (Wang et al., 2015; Fang et al., 2019; Jin et al., 2020; Zhao et al., 2020; Gu et al., 2022; Qiu et al., 2022). These results suggest that the enrichment of organic matter in the shale of the Lower Cambrian Qiongzhusi Formation may have been controlled by a variety of interrelated geological and geochemical processes, which leads to complicated enrichment mechanisms of organic matter (Xia et al., 2020). Moreover, in previous studies, the mechanisms of organic matter enrichment were often only discussed in the passive continental margin (such as the slope facies in northern Guizhou and western Hunan Province) or craton depression areas (such as the deep-water shelf facies in western Sichuan or western Hubei Province). There is a lack of systematic comparison between the different sedimentary backgrounds, resulting in major differences between the reported main controlling factors and formation mechanisms and unclear explanations of the different mechanisms of organic matter enrichment across different regions.

Consequently, we researched the Sichuan Basin and the Lower Cambrian Qiongzhusi Formation via sample collection mainly from Duodingguan in Weng'an and Morong in Guzhang along the passive continental margin area, Baizhuling in Changyang and well YD2 in the Western Hubei Trough area, and well W201 in the western Sichuan Trough area (Fig. 1(a) and (b)). Organic matter content and element analysis data were used to analyze the sedimentological and geochemical characteristics of the shale strata. The characteristics and variation trends of the depositional paleoenvironment of the Qiongzhusi Formation in the passive continental margin, the western Sichuan Trough, and the western Hubei Trough were systematically investigated. Furthermore, the main factors controlling the differences in the organic matter enrichment across different regions were clarified, and a corresponding enrichment model was established to enhance our understanding of the geological environment of the organic matter enrichment during the E-C transitional period.

2. Geologic setting

Tectonic activity was frequent and the tectonic environment was complex in the Sichuan Basin during the Cambrian (Fan et al., 2021). In the Early Cryogenian, the breakup of the Rodinia supercontinent was occurring, and rift basins formed in the western part of the Middle Yangtze and Upper Yangtze paleo-continents under the global extensional tectonic background. Based on the landform inheritance of the low-lying tectonic units, the West Sichuan Trough and the Western Hubei Trough formed under the influence of the extensional activity during the Sinian-Early Cambrian (Fig. 1(a) and (b)) (Wang et al., 2015; Ma et al., 2019; Fan et al., 2021; Xie, 2021). The evolution of the trough within the Yangtze Plate mainly occurred as follows: 1) the uplift and denudation stage (the end of the Dengying Formation); 2) the initial extensional stage (Yanjiahe/Maidiping Period), during which extensional activity began and thick strata rich in silica-phosphorus were deposited; 3) the extensional peak stage (the early phase of the Qiongzhusi Formation), during which the sea level rose rapidly, the transgression range expanded rapidly, and a series of massive, thick black rocks were deposited in the center of the extensional trough; and 4) the extensional weakening stage (the end of Qiongzhusi-Shipai/Canlangpuan), during which there was shallower water deposition, infilling of detrital materials in the trough, and the disappearance of the uplift-sag pattern in the Yangtze region (Fig. 1(c)) (Liu et al., 2015, 2016; Xie, 2021).

Within the study area, there are well-developed Lower Cambrian strata. From bottom to top, they include the Yanjiahe/Maidiping Formation, Qiongzhusi Formation, and Shipai/Canglangpu Formation. Among these strata, the Yanjiahe/Maidiping Formation is dominated by phosphorus-bearing siliceous rocks, phosphate-block rocks, and phosphorus-bearing carbonate rocks, which conformably overlie the algal dolomites of the Dengying Formation in the Lower Sinian System. The Qiongzhusi Formation conformably overlies the Yanjiahe Formation and is unconformably overlain by the Dengying Formation (Wang et al., 2015). From bottom to top, this formation can be divided into three members (hereinafter referred to as Q1, Q2, and Q3). overall, organic matter content, biogenic silica, and gamma-ray (GR) log values exhibited decreasing trends, while the content of gray/silty material exhibited a gradually increasing trend, and the lithology gradually transitioned from black carbonaceous-siliceous shale to gray-white gray/silty shale. The Shipai/Canglangpu Formation, dominated by clayey shale and marly/sandy shale deposits, is in conformable contact with the Qiongzhusi Formation (Fig. 1(c)) (Wu et al., 2020a; He et al., 2021). The results of paleogeographic restoration show that during the depositional periods of the Qiongzhusi Formation, the Yangtze Plate was located near the paleo-equator (Zhang et al., 2005), with the ocean on the west side and the passive continental margin slope opening to the east on the east side. The sedimentary sequence was well-developed from southeast to northwest in the following order: basin facies, slope facies, deep-water shelf facies, and shallow shelf facies (Fig. 1(a)) (Liu et al., 2017). Marine shale is widely distributed in the Yangtze region, and the thicknesses of the
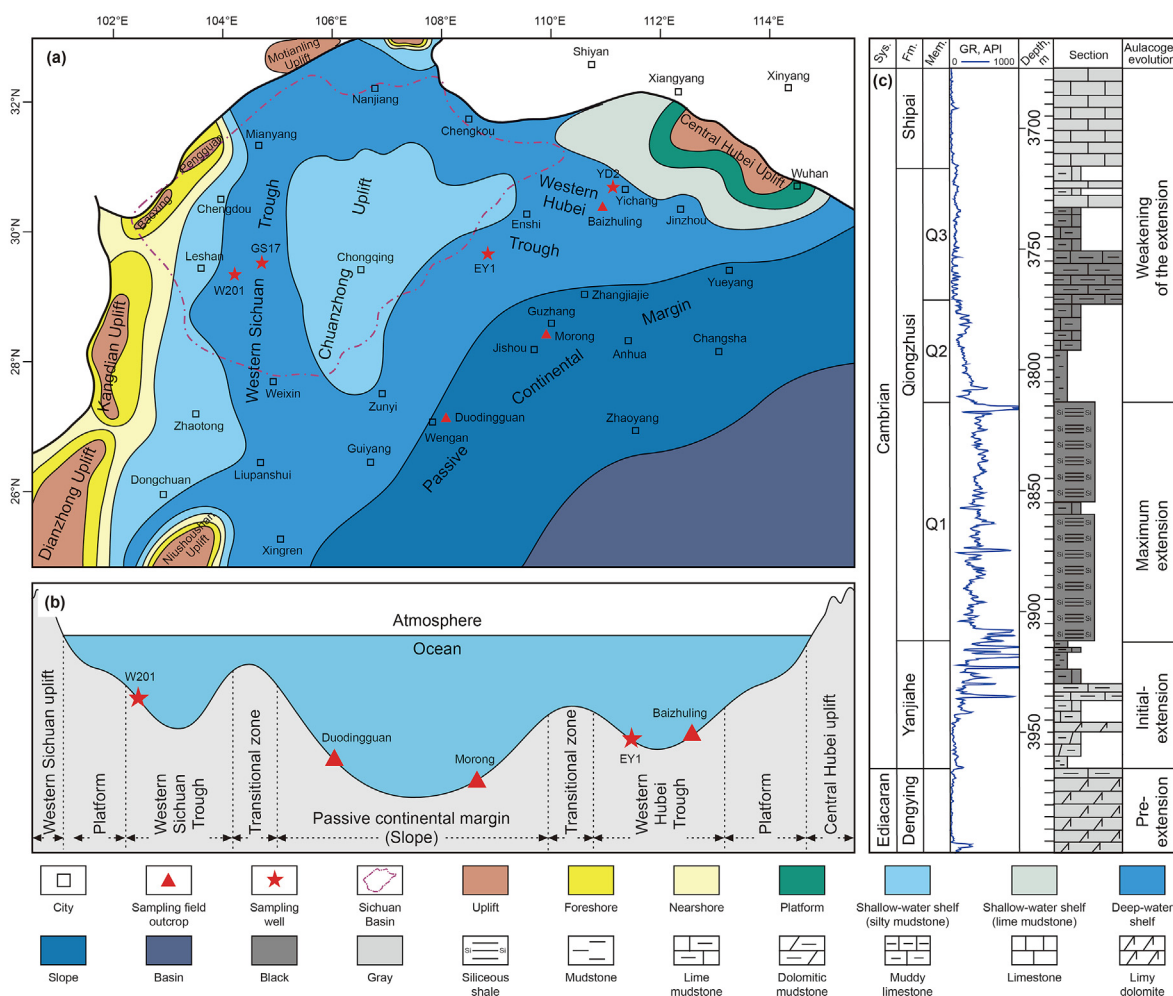
Fig. 1. **(a)** Map of the paleogeography of the Early Cambrian Qiongzhusi lithofacies in the Sichuan Basin and its periphery (modified from Ma et al., 2009); **(b)** cross-sections through the western Sichuan Trough, passive continental margin, and western Hubei Trough in the study area; and **(c)** histogram of stratigraphy and rift evolution of the Qiongzhusi Formation in the study area (from Well EY1).

organic-rich shale are greater in the western Sichuan Trough and the western Hubei Trough than in the passive continental margin area (Zhao et al., 2016).

3. Materials and methods

3.1. Samples

A total of 234 samples were collected from the black shale section of the Qiongzhusi Formation, including 33 black shale samples from well W201 in the western Sichuan Trough. In addition, 119 black shale samples were collected from the western Hubei Trough, including 52 samples from the Baizhuling section in Changyang and 67 samples from well YD2. A total of 82 black shale samples were collected along the passive continental margin, including 28 samples from the Morong section in Guzhang and 54 samples from the Dudingguan section in Weng'an. The organic carbon content, mineral petrological characteristics, and micropaleontological features of these samples were analyzed. Based on the results of these analyses, 28, 16, and 13 samples were further selected from well W201, Baizhuling, and Duodingguan for element analysis.

3.2. Analytical methods

The analysis and testing of all of the black shale samples discussed in this paper were completed by the geological laboratory of the Exploration and Development Research Institute of the Petro-China Southwest Oil & Gas Field Branch. The organic matter abundance test was completed using an ELTRA CS-580A carbon and sulfur tester (Germany). First, the samples were washed with deionized water and manually ground to 80 mesh using an agate mortar. Then 100 mg of sample were weighed, dissolved in 5% HCl, and left to soak for 24 h to remove inorganic carbon such as carbonates. The organic carbon content was analyzed. The analysis accuracy was ±0.5%, and the instrument used for the X-diffraction analysis was a Philips PW1830 X-ray diffractometer. The powdered sample was placed in the diffractometer, smoothed, and pressed to remove the excess, after which, the prepared sample was scanned by Cu-Ka rays to obtain the diffraction spectrum. Finally, the mineral species were determined according to the 2θ angle (scanning range of $20°-40°$) and the spectral peak intensity. Shale samples weighing about 1 g were placed in a clean ceramic crucible, and the weights of the crucible, sample, and crucible + sample were measured and recorded. The crucible was calcined in a muffle
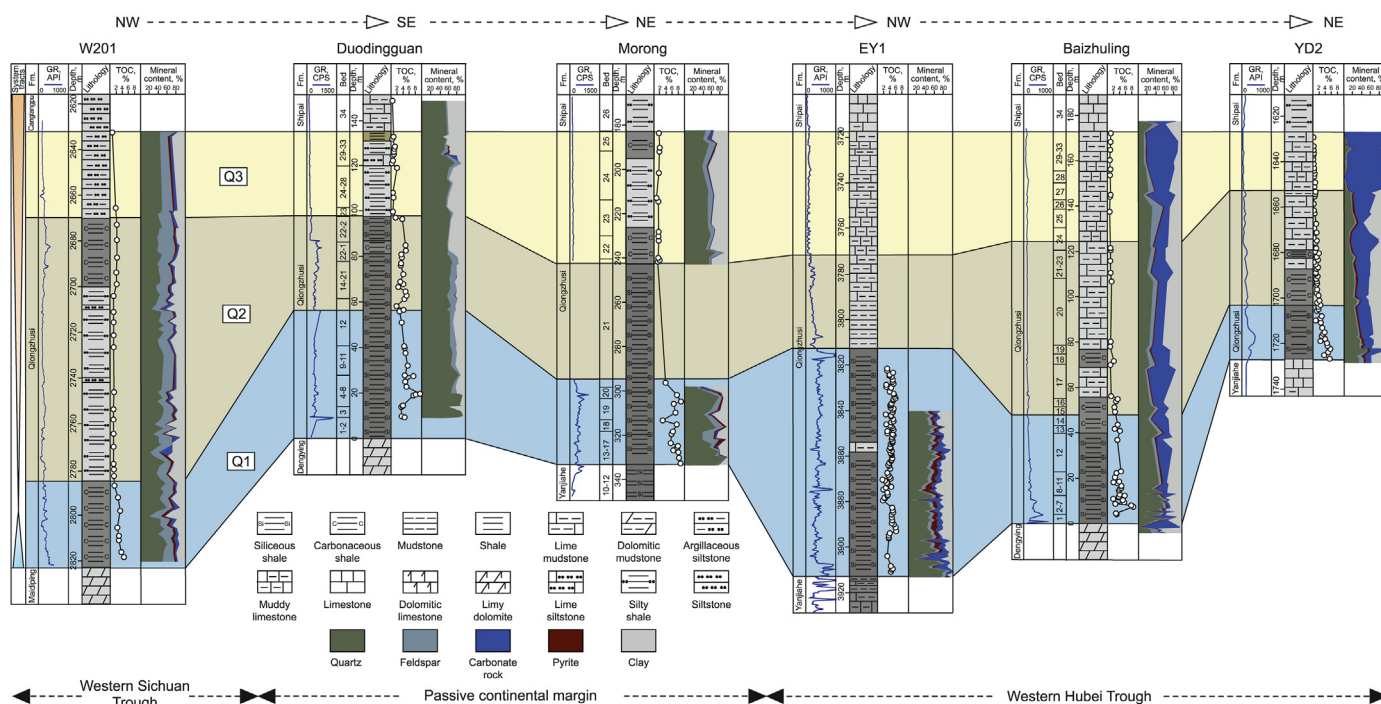
Fig. 2. Stratigraphic comparison of the Lower Cambrian Qiongzhusi Formation in the passive continental margin, the western Hubei Trough, and the western Sichuan Trough and the sedimentary filling characteristics in different periods. The natural gamma data for the Duodingguan, Morong, and Baizhuling outcrops were measured using an HD-2000 handheld radiometer, produced by the Instrument Research and Development Institute of Beijing Institute of Geology, Nuclear Industry, with a test interval of 0.2—0.5 m. The cps denotes counts per second. The vegetation cover in the Q2 section of the Morong section was severe, and no natural gamma data were measured.

furnace at 920 °C for 3—4 h to remove the organic matter and carbonates, after which it was removed, quickly placed on a drying dish to cool, and weighed at room temperature to determine the weight reduction. About 0.5 g of each ground sample was weighed after heating. Then, an amount of $Li_2B_4O_7$ equivalent to about 8 times the sample mass was added, evenly mixed, melted into glass sheets, and tested using a Rigaku 100e wavelength dispersive X-ray fluorescence spectrometer (XRF). The trace elements were analyzed and tested using a Thermo Scientific Element XR Inductively Coupled Plasma Mass Spectrometer (Germany). About 50 mg of each baked shale sample were accurately weighed and placed into a clean Teflon container, and 3 mL of HNO_3, 3 mL HF, and 1.5 mL of $HClO_4$ were added to dissolve the sample. The samples were sonicated for 1 h until they were evenly mixed, heated on a temperature hot plate at 100 °C for 3 days, and evaporated to until dry. After this, 1 mL of HNO_3 and 3 ml of HF were added, the beaker was resealed and heated at 180 °C for 48 h until the residue was completely dissolved, and the concentrated solution was transferred to a polyethylene bottle and diluted to 100 mL with 2% HNO_3. Each diluted sample was dissolved and analyzed on a PE Elan6000 inductively coupled plasma mass spectrometer (ICP-MS), with an analytical error of less than 5%.

3.3. Data presentation

The degree of enrichment of an element in sediments is generally expressed as the enrichment coefficient (EF) to exclude terrigenous inputs and other factors (Tribovillard et al., 2006).

$$X_{EF} = (X/Al)_{sample}/(X/Al)_{PAAS,} \tag{1}$$

Where X and Al are the amounts of X and Al in a sample, and the sample is standardized in reference to Post-Archean Australian shale (PAAS).

The C_{org}/P value in the C-S-FE-P system is often used to indicate the redox conditions of the water (Algeo and Liu, 2020), and it is calculated as follows:

$$C_{org}/P = (\text{organic carbon content}/\text{ molar mass of an element C}) / (\text{element content P / molar mass of element P}). \tag{2}$$

Since most sedimentary rocks have both biological and terrigenous inputs, the content of the biological origin of the elements is often used to evaluate the level of paleo-productivity. The biological content (X_{XS}) is calculated as follows (Murray and Leinen, 1996; Tribovillard et al., 2006):

$$X_{XS} = X_{sample} - Al_{sample} (X/Al)_{PAAS,} \tag{3}$$

Where X_{sample} and Al_{sample} are the total contents of elements X and Al, respectively, and $(X/Al)_{PAAS}$ is the ratio of these two elements relative to PAAS.

4. Results

4.1. Organic carbon content

The total organic carbon (TOC) content of the Qiongzhusi Formation in the study area varied significantly across different regions in different periods. The TOC content of Q1 in the passive continental margin was 2.8%—9.5%, with an average of 5.8%. The TOC content of Q2 was 1.4%—5.0%, with an average of 3.6%. The TOC content of Q3 was 0.2%—2.0%, with an average of 0.8%. In the western Hubei Trough area, the TOC contents of Q1, Q2, and Q3 were 1.3%—8.5%, 0.2%—3.3%, and 0.01%—1.1%, with averages of 3.9%, 1.2%, and 0.5%, respectively. In the western Sichuan Trough area, the

Table 1
Calculated major and trace element compositions for the Qiongzhsi Formation in the study area.

Zone	Section	Fm.	Depth, m	TOC, %	Al_2O_3, %	Al_2O_3+MgO + CaO, %	Al, %	Si, µg/g	K, µg/g	Co, µg/g	Ni, µg/g	U, µg/g	Th, µg/g	Mo, µg/g
Passive continental margin	Duodingguan	Q3	19.4	0.4	18.9	20.9	10.0	295631.8	33687.5	5.0	20.6	5.9	8.1	2.9
			26.2	0.9	17.9	21.9	9.5	281383.1	30690.7	17.8	53.2	6.0	5.9	2.8
			38.2	0.4	17.6	20.6	9.3	284998.2	31852.9	14.0	55.3	6.6	7.5	5.4
		Q2	54.7	3.7	16.1	17.9	8.5	318533.9	32517.0	2.5	19.6	52.4	5.5	40.9
			74.1	3.2	15.4	16.6	8.2	331124.8	26979.9	1.0	16.4	78.0	9.9	28.9
			82.1	3.0	15.5	17.0	8.2	312648.4	29304.3	1.5	9.5	35.4	4.9	42.8
			92.9	1.8	15.1	16.5	8.0	313615.5	30541.2	1.3	11.3	70.7	10.4	78.5
		Q1	110.1	3.9	12.8	13.9	6.8	317090.1	27976.1	3.3	90.0	21.3	12.6	30.1
			113.4	4.7	11.8	13.0	6.2	341145.9	27760.2	2.1	44.3	24.2	3.7	52.2
			119.1	5.0	11.6	12.8	6.1	313543.2	26730.8	2.1	53.5	28.4	9.4	44.4
			126.0	4.4	11.0	12.0	5.8	319580.7	25070.5	3.0	92.7	27.7	9.9	33.1
			131.4	8.2	8.9	9.9	4.7	355965.7	22937.1	2.1	71.7	43.8	6.3	102.3
			136.5	3.8	6.0	6.6	3.2	397625.2	13622.8	0.5	5.6	15.7	4.5	36.8
Western Hubei trough	Baizhuling	Q3	5.8	1.1	14.3	23.6	7.6	270315.6	22289.5	15.8	43.6	5.1	10.3	5.2
			13.0	0.9	5.5	47.4	2.9	135932.7	6923.5	4.9	29.4	4.7	3.2	5.8
			17.6	0.8	5.9	46.1	3.1	136097.0	7687.2	4.5	21.4	3.5	3.5	3.7
			33.8	0.8	9.6	36.3	5.1	187866.1	13099.8	9.2	37.9	5.4	6.6	7.2
			35.4	0.4	8.7	46.5	4.6	138352.9	12087.0	8.2	31.7	3.4	6.0	2.7
		Q2	57.6	1.1	13.8	28.7	7.3	245900.9	21351.5	14.9	53.0	5.4	10.3	5.7
			67.6	1.0	7.9	40.7	4.2	159232.8	10302.2	7.2	32.6	4.9	5.6	4.6
			71.3	1.3	12.9	27.2	6.9	254604.6	19940.2	13.5	48.2	5.7	10.1	6.7
			99.9	0.9	11.1	36.8	5.9	202240.5	16370.6	10.3	39.1	5.6	7.6	9.2
			106.2	2.0	10.2	32.3	5.4	216304.0	14859.7	10.8	42.7	8.0	7.7	8.4
			107.9	1.0	5.9	48.0	3.1	134365.2	7952.8	5.6	29.9	5.4	3.6	9.3
			124.0	2.8	10.7	21.8	5.7	290578.3	17366.7	10.2	50.7	8.8	8.8	21.0
		Q1	134.3	3.3	11.5	20.5	6.1	292940.7	18836.1	12.3	61.4	12.0	9.2	29.4
			141.0	3.2	9.6	30.5	5.1	242641.5	14212.2	9.6	31.0	11.9	8.1	10.3
			162.2	4.5	10.3	13.6	5.4	338772.7	17790.1	17.1	164.9	21.1	6.8	59.8
			166.7	5.6	10.8	12.6	5.7	346623.7	22380.8	2.6	29.2	17.0	5.1	46.6
Western Sichuan trough	W201	Q3	2631.3	0.8	12.3	17.0	6.5	313322.8	24489.4	11.3	32.6	4.3	11.8	2.1
			2665.6	2.0	14.4	20.1	7.6	283921.1	29387.3	17.9	72.6	11.6	11.3	13.7
		Upper part of Q2	2679.6	2.4	12.6	16.6	6.7	292101.2	24738.5	22.1	149.0	29.3	14.2	45.0
			2687.3	2.4	14.2	19.8	7.5	287754.0	27145.9	15.6	65.3	13.0	12.4	16.9
			2693.8	2.2	13.4	19.4	7.1	284996.2	25402.6	22.4	79.0	14.7	12.6	19.2
			2698.9	2.3	13.9	20.0	7.4	279760.9	26813.9	17.4	39.5	8.9	11.4	13.0
		Middle and lower part of Q2	2704.1	1.3	13.9	19.8	7.3	287847.5	25734.7	17.5	54.7	7.4	12.4	9.9
			2711.1	1.3	12.1	18.8	6.4	299954.1	20919.8	12.5	35.6	6.5	10.8	7.7
			2715.6	1.3	12.2	18.7	6.4	304441.5	20338.7	11.4	27.0	5.2	11.5	4.3
			2721.3	1.3	12.8	19.4	6.8	293410.0	22082.0	14.5	34.0	4.6	12.2	5.2
			2726.5	1.3	12.5	21.2	6.6	280321.8	21583.9	14.6	32.8	6.1	11.1	6.9
			2746.1	1.4	14.4	19.3	7.6	286959.4	27228.9	20.0	67.9	11.2	13.1	13.3
			2753.6	1.3	13.8	19.2	7.3	290979.4	25900.7	18.3	83.2	15.4	11.5	22.4
			2758.1	1.3	14.2	18.4	7.5	295186.3	25983.7	19.1	76.6	13.7	12.8	17.4
			2764.3	1.3	17.6	21.6	9.3	268822.9	35281.4	32.5	92.7	13.1	14.5	16.6
			2770.0	1.3	12.7	16.5	6.7	324073.9	19757.6	15.9	28.9	3.2	9.5	3.3
			2777.5	1.3	16.4	20.8	8.7	276956.3	32458.9	18.5	88.6	15.6	16.2	34.3
			2779.9	1.4	13.7	19.3	7.3	298785.5	23410.2	17.1	56.4	7.7	13.7	4.3
			2782.8	1.4	15.7	19.9	8.3	289296.6	29968.4	19.8	70.3	10.0	14.7	12.0
		Q1	2787.0	1.6	15.2	19.4	8.0	285977.8	29636.4	19.3	99.6	24.1	14.1	31.5
			2792.2	2.7	13.7	18.2	7.2	291727.3	27644.0	17.5	116.0	17.8	11.5	24.2
			2798.0	3.4	11.5	19.5	6.1	285931.0	24074.4	16.8	83.2	21.0	10.5	31.2
			2805.4	2.5	13.6	19.0	7.2	281583.9	33289.0	19.3	113.0	20.1	12.5	42.6
			2809.0	3.0	13.9	19.0	7.3	285790.8	33123.0	19.7	93.6	20.5	12.1	25.2
			2811.0	3.0	13.0	18.7	6.9	296214.6	30217.5	18.3	115.0	17.5	11.4	23.7
			2816.1	3.8	11.8	17.7	6.2	289670.5	28889.2	18.4	132.0	47.7	9.8	72.7
			2818.3	4.7	12.3	17.0	6.5	288548.7	30466.5	16.2	120.0	29.6	9.7	52.5

Note:/means that the calculated value is negative and thus was eliminated during the actual application.

TOC contents of Q1 and Q2 were 1.1%−6.4% and 0.3%−4.5%, with averages of 2.8%, and 1.8%: however, the high-quality shale section had a content of more than 2%, mainly in the upper part of the section, with an average of 2.2%. The TOC content of Q3 was 0.3%−2.0%, with an average of 0.6% (Fig. 2; Table 1).

In general, the TOC contents of the sample along the passive continental margin and from the western Hubei Trough area decreased significantly in the longitudinal direction from Q1 to Q2 to Q3. Although the TOC content of the upper part of Q2 in the West Sichuan Trough area increased (Fig. 2; Table 1), this trend was still maintained. In the latitudinal direction, the TOC contents decreased from the passive continental margin to the craton depression, and the TOC content was greater in the western Hubei Trough area than in the western Sichuan Trough in the Q1 period. By the end of Q2, the TOC was lower than that in the western Sichuan Trough at the end of Q1, and there were no significant differences from the other periods.

4.2. Sedimentological and petrological characteristics

Q1: The passive continental margin was dominated by black siliceous sediments, with undeveloped internal striations and

P, µg/g	Ba, µg/g	Mn, µg/g	K/Al	C_{org}/P	U/Th	Ni/Co	U_{EF}	Mo_{EF}	$Si_{xs} \times 10^{-4}$, µg/g	$Ba_{xs} \times 10^{-2}$, µg/g	$P/Al \times 10^4$	Mo/TOC	$Co_{EF} \times Mn_{EF}$
268.7	810.5	143.4	0.34	37.5	0.7	4.2	1.9	2.9	/	1.6	26.8	7.5	0.04
481.9	684.2	508.5	0.32	47.7	1.0	3.0	2.0	3.0	/	0.7	51.0	3.2	0.52
362.8	1101.0	325.5	0.34	29.2	0.9	3.9	2.3	5.8	/	4.9	38.9	13.2	0.27
236.1	1653.0	93.1	0.38	401.9	9.5	7.8	19.9	48.1	5.4	11.0	27.8	11.1	0.02
409.7	1857.1	62.9	0.33	204.9	7.9	16.1	30.9	35.5	7.7	13.3	50.2	8.9	0.00
497.7	971.4	167.3	0.36	155.4	7.2	6.2	13.9	52.1	5.7	4.4	60.5	14.3	0.02
533.1	1171.2	290.2	0.38	85.8	6.8	8.9	28.6	98.2	6.5	6.5	66.7	44.3	0.03
712.6	3540.9	24.0	0.41	141.4	1.7	27.2	10.2	44.5	10.7	31.0	105.4	7.7	0.01
351.7	4558.9	131.4	0.45	344.4	6.5	21.2	12.6	83.9	14.8	41.5	56.5	11.1	0.04
842.1	3676.2	24.6	0.44	154.6	3.0	25.4	15.0	72.6	12.3	32.8	137.6	8.8	0.01
712.6	1847.6	31.6	0.43	158.8	2.8	30.5	15.4	57.1	13.9	14.7	123.0	7.6	0.01
508.2	2273.2	161.5	0.49	414.9	7.0	34.7	29.9	216.6	20.9	19.7	107.7	12.5	0.08
764.4	680.0	349.0	0.43	129.4	3.5	10.6	16.0	116.5	29.9	4.7	242.3	9.6	0.09
567.0	1557.6	318.7	0.29	50.2	0.5	2.8	2.2	6.8	3.4	10.6	74.7	4.7	0.45
307.4	457.7	259.1	0.24	78.3	1.5	6.0	5.2	19.8	4.5	2.7	105.3	6.2	0.76
362.0	459.0	296.8	0.25	55.0	1.0	4.7	3.6	12.0	3.9	2.6	116.5	4.8	0.71
452.8	740.8	612.3	0.26	47.3	0.8	4.1	3.4	14.2	3.0	4.1	89.1	8.7	1.11
364.9	774.9	757.9	0.26	31.5	0.6	3.9	2.4	5.9	/	4.8	79.4	6.1	1.51
547.0	1219.3	480.6	0.29	50.0	0.5	3.6	2.4	7.9	1.9	7.5	75.0	5.4	0.69
535.4	688.7	628.0	0.25	48.6	0.9	4.5	3.8	11.0	2.9	4.2	127.7	4.6	1.32
523.9	1156.3	417.1	0.29	65.8	0.6	3.6	2.7	9.7	4.2	7.1	76.5	5.0	0.61
355.0	1275.4	795.9	0.28	66.1	0.7	3.8	3.1	15.7	1.9	8.9	60.4	10.2	1.21
397.9	1041.2	490.9	0.27	133.0	1.0	3.9	4.8	15.5	4.8	6.9	73.5	4.1	0.93
372.4	1096.4	300.7	0.26	66.8	1.5	5.3	5.6	29.8	3.8	8.9	119.9	9.6	0.90
535.7	1191.1	484.9	0.31	135.1	1.0	5.0	5.0	37.1	11.4	8.2	94.5	7.5	0.79
447.2	1457.9	239.1	0.31	191.2	1.3	5.0	6.4	48.6	10.4	10.6	73.8	8.9	0.41
359.1	2103.2	325.0	0.28	232.4	1.5	3.2	7.6	20.4	8.5	17.7	70.8	3.2	0.62
543.9	2365.2	135.7	0.33	211.3	3.1	9.7	12.5	110.0	17.0	20.1	100.1	13.4	0.40
260.6	2135.1	101.6	0.39	558.9	3.4	11.3	9.6	81.8	16.9	17.6	45.7	8.3	0.04
1475.1	919.0	426.0	0.37	14.4	0.4	2.9	2.1	3.2	11.0	4.9	225.9	2.6	0.58
1182.7	1113.0	472.4	0.39	42.8	1.0	4.1	4.9	18.0	4.7	6.2	155.4	7.0	0.75
1326.7	1071.0	340.8	0.37	46.1	2.1	6.7	14.2	67.4	8.5	6.4	198.8	19.0	0.86
2003.2	957.0	418.2	0.36	31.3	1.0	4.2	5.6	22.6	5.5	4.7	267.5	7.0	0.60
1147.8	930.0	480.2	0.36	48.8	1.2	3.5	6.7	27.1	6.4	4.7	161.7	8.8	1.09
960.1	899.0	449.2	0.36	61.9	0.8	2.3	3.9	17.7	5.1	4.2	130.6	5.7	0.74
968.9	899.0	472.4	0.35	34.1	0.6	3.1	3.2	13.5	6.0	4.2	132.1	7.7	0.79
1182.7	1028.0	619.6	0.33	28.0	0.6	2.8	3.3	12.0	10.0	6.1	184.2	6.0	0.96
1213.3	964.0	573.1	0.32	27.7	0.4	2.4	2.6	6.6	10.4	5.5	188.4	3.3	0.81
1095.4	859.0	588.6	0.32	30.9	0.4	2.3	2.2	7.7	8.2	4.2	161.2	4.0	0.95
1213.3	853.0	751.2	0.33	27.9	0.5	2.2	3.0	10.5	7.5	4.2	184.1	5.3	1.29
1082.3	1102.0	364.0	0.36	33.7	0.9	3.4	4.7	17.5	5.0	6.1	142.2	9.4	0.64
1130.4	938.0	449.2	0.35	28.6	1.3	4.5	6.8	30.6	6.3	4.6	154.4	17.9	0.78
1160.9	876.0	333.0	0.35	28.0	1.1	4.0	5.9	23.2	6.2	3.9	154.6	13.8	0.58
1235.1	1083.0	263.3	0.38	26.6	0.9	2.9	4.5	17.9	/	4.8	132.8	13.1	0.51
1387.8	848.0	333.0	0.29	23.8	0.3	1.8	1.6	4.9	11.6	4.1	207.1	2.6	0.60
1008.2	1108.0	302.0	0.37	33.1	1.0	4.8	5.8	39.5	0.7	5.4	116.2	26.6	0.38
1121.6	974.0	418.2	0.32	31.8	0.6	3.3	3.4	6.0	7.3	5.0	154.5	3.1	0.69
1252.6	1039.0	294.3	0.36	28.9	0.7	3.6	3.9	14.4	3.1	5.0	150.5	8.6	0.43
1108.5	1074.0	340.8	0.37	36.6	1.7	5.2	9.7	39.2	3.6	5.5	138.1	20.1	0.52
1174.0	1006.0	379.5	0.38	59.9	1.5	6.6	7.9	33.5	6.7	5.4	162.5	8.9	0.65
947.1	1173.0	534.4	0.39	93.8	2.0	5.0	11.1	51.2	9.6	7.8	155.3	9.1	1.24
916.5	1611.0	379.5	0.46	70.5	1.6	5.9	9.0	59.2	5.8	11.4	127.4	17.0	0.72
964.5	1551.0	317.5	0.45	80.9	1.7	4.8	9.0	34.3	5.7	10.7	131.4	8.3	0.59
1187.1	1580.0	348.5	0.44	65.1	1.5	6.3	8.2	34.5	8.3	11.3	172.8	7.9	0.69
903.4	1752.0	387.2	0.46	109.5	4.9	7.2	24.7	116.6	9.6	13.5	144.9	19.0	0.94
894.7	1725.0	309.8	0.47	135.1	3.1	7.4	14.7	80.7	8.6	13.0	137.5	11.2	0.61

microfossils mainly consisting of radiolarians (Fig. 3(a), 4(a) and 4(b)). The quartz content was the highest in the entire region (64.4% on average), and most of the quartz grains were sub-rounded micro-silt crystalline particles with a biogenic origin. The feldspar (5.5% on average), carbonate rocks (2.4% on average), and clay minerals (15.7% on average) had low contents. The western Hubei Trough was dominated by grayish-black siliceous shale, and the microfossils were predominantly radiolarians (Fig. 3(b), 4(g) and 4(h)). The quartz content (38.5% on average) was significantly lower compared with that in the passive continental margin. However, the contents of the carbonates (21.3% on average, the highest in the entire region) and clay minerals (26.1% on average) were significantly higher, and

the feldspar content (6.4% on average) was lower and did not change significantly (Fig. 2). Within the western Sichuan Trough area, the lithology was dominated by siliceous shale deposits (Fig. 3(c)). Sandy veins were not observed in the hand specimens (Fig. 4(m)); however, weakly developed striations were observed under the microscope (Fig. 4(n)). The quartz content was high (45.1% on average), and the quartz mainly consisted of sub-rounded particles with a biogenic origin and subangular particles with a terrigenous origin (Fig. 4(n)). The feldspar content (21.2% on average) was the highest in the region (Fig. 2), which was closely related to the high terrigenous input in this area (Guo, 2023) and was the main reason for the co-occurrence of biogenic and terrigenous silica in the deep-water
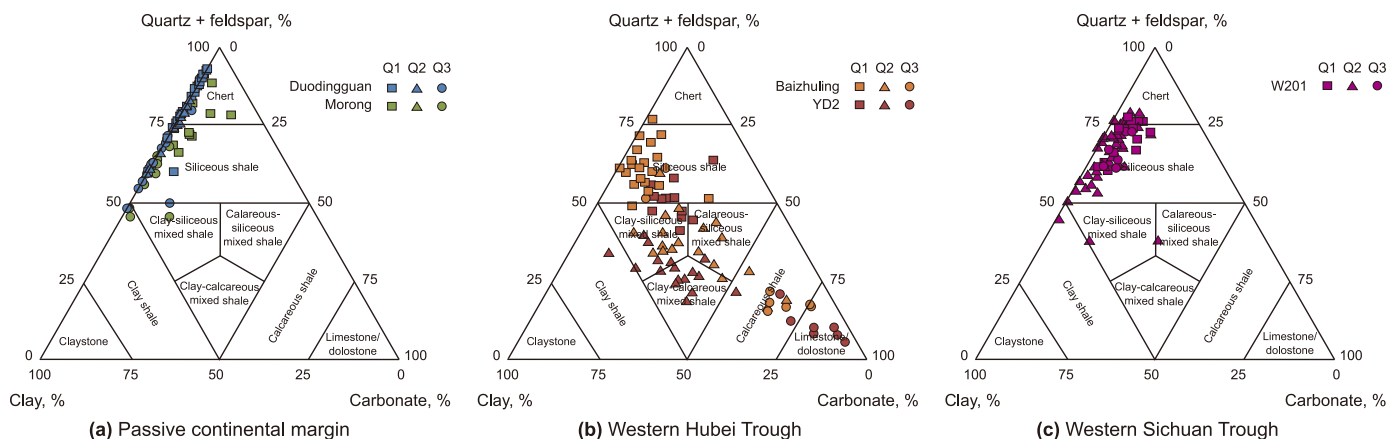
Fig. 3. Ternary plots of rock types from different depositional periods of the Qiongzhusi Formation: **(a)** passive continental margin, **(b)** western Hubei Trough, and **(c)** western Sichuan Trough.

environment. The clay mineral content (average 23.1%) was medium, and the carbonate content was low (average 5.5%). The lithofacies with these characteristics are henceforth referred to as carbonaceous shale to facilitate distinction from the biogenic siliceous shale.

Q2: The passive continental margin was dominated by inter-bedded gray-black siliceous rocks and siliceous shale deposits. The quartz content (average 62.1%) in this site was still the

Highest in the entire region, and a large number of siliceous bioclasts and radiolarian microfossils were observed under the microscope (Fig. 3(a), 4(c) and 4(d)). The contents of the feldspar (average 12.9%) and clay minerals (average 24.2%) were higher than those in Q1, and the carbonate rock content (average 0.2%) remained low. The western Hubei Trough mainly consisted of a mixture of gray-black clay, siliceous, and calcareous shale sediments (Fig. 3(b)), and the quartz content (average 21.7%) was significantly lower than that in Q1. The content of the carbonate rocks (38.2% on average) was significantly higher (the highest values of the entire area) (Fig. 2). The carbonate rocks occurred as striated layers in the outcrop and were mainly distributed in the form of speckled layers in the organic-rich clayey matrix under the microscope (Fig. 4(i) and (j)). The content of the clay minerals (32.1% on average) was higher than that in Q1, and the content of feldspar was lower (4.0% on average). The lithologic characteristics exhibited a clear contrast after entering the western Sichuan Trough area, with dark gray silty shale sediments in the middle and lower parts, and many horizontal sandy layers in the hand specimens and microscopic sections (Fig. 4(o)). The contents of the quartz (39.0% on average), feldspar (23.3% on average), and clay minerals (29.9% on average) were relatively high, and the feldspar content was the highest in the region, while the carbonate content was low (4.7% on average) (Fig. 2). The upper part was dominated by grayish-black carbonaceous shale deposits (Fig. 3(c)), and pyrite clumps were observed in the hand specimens with undeveloped sandy layers (Fig. 4(p)). The contents of the quartz (39.4% on average; both biogenic and terrigenous particles were visible; Fig. 4(p)) and feldspar (31.1% on average) were relatively high, the content of the clay minerals was moderate (21.9% on average), and the content of the carbonate rocks was low (4.1%).

Q3: The passive continental margin was dominated by dark gray silty shale deposits. The quartz (average 53.1%) was mainly terrigenous (Fig. 4(e) and (f)). The content of the clay minerals (average 36.1%) was significantly higher than that during Q2,

and the contents of the feldspar (average 8.0%) and carbonate rock (average 1.6%) were lower. The western Hubei Trough was dominated by argillaceous limestone, and the contents of the quartz (11.7% on average) and clay minerals (10.4% on average) were significantly lower compared with Q2, while the carbonate content (71.3% on average) increased significantly (Fig. 2), with a large number of calcareous bands (Fig. 4(k) and (l)), and the feldspar content was low (5.1% on average). After entering the western Sichuan Trough, the lithology was dominated by argillaceous siltstone with developed fine silt bands (Fig. 4(q) and (r)) of quartz (41.6% on average), feldspar (23.3% on average), and clay minerals (26.0% on average). The carbonate rock content was low (6.0% on average).

5. Discussion

5.1. Terrigenous input

The chemical properties of K and Al in sediments are very stable, rarely affected by weathering and diagenesis, usually only found in aluminosilicate minerals such as clay minerals, and generally transported to sedimentary basins by fluvial or aeolian processes (Murphy et al., 2000). Therefore, the Al_2O_3 content and K/Al values are often used to assess terrigenous inputs in sediments (Pedersen and Calvert, 1990; Murphy et al., 2000; Algeo and Liu, 2020). The terrigenous input is generally in the form of debris flows, which are mainly controlled by the relative sea level where there is landward flow during transgression and to the interior of the basin during marine regression (Lu et al., 2019). From Q1 to Q3, the sea level continued to decrease, the rifting gradually weakened (Liu et al., 2016), the Al_2O_3 content in the passive continental margin area (averages: 10.3% (Q1) → 15.5% (Q2) → 18.1% (Q3)) increased, and the K/Al values (averages: 0.44→0.36→0.33) decreased, indicating that the terrigenous input increased. In the western Hubei Trough, the supply of terrigenous clasts (mostly calcareous clasts) mainly came from the carbonate paleo-continental rocks in the Dengying Formation in central Hubei Province (Wang et al., 2021; Liu et al., 2022b; Guo, 2023). As such, the content of Al_2O_3 (10.5% → 10.4%→8.8%) could not accurately indicate variations. However, the influence of the carbonate rocks on the increased $Al_2O_3+MgO + CaO$ content (averages: 19.3%→33.6%→40.0%) was considerable (Table 1, Figs. 2 and 5). This is corroborated by the changes in the K/Al values (0.33→0.28→0.26) and mineral characteristics (Fig. 4). Upon entering the western Sichuan Trough, from Q1→the lower middle part of Q2→the upper part of Q2→Q3, the
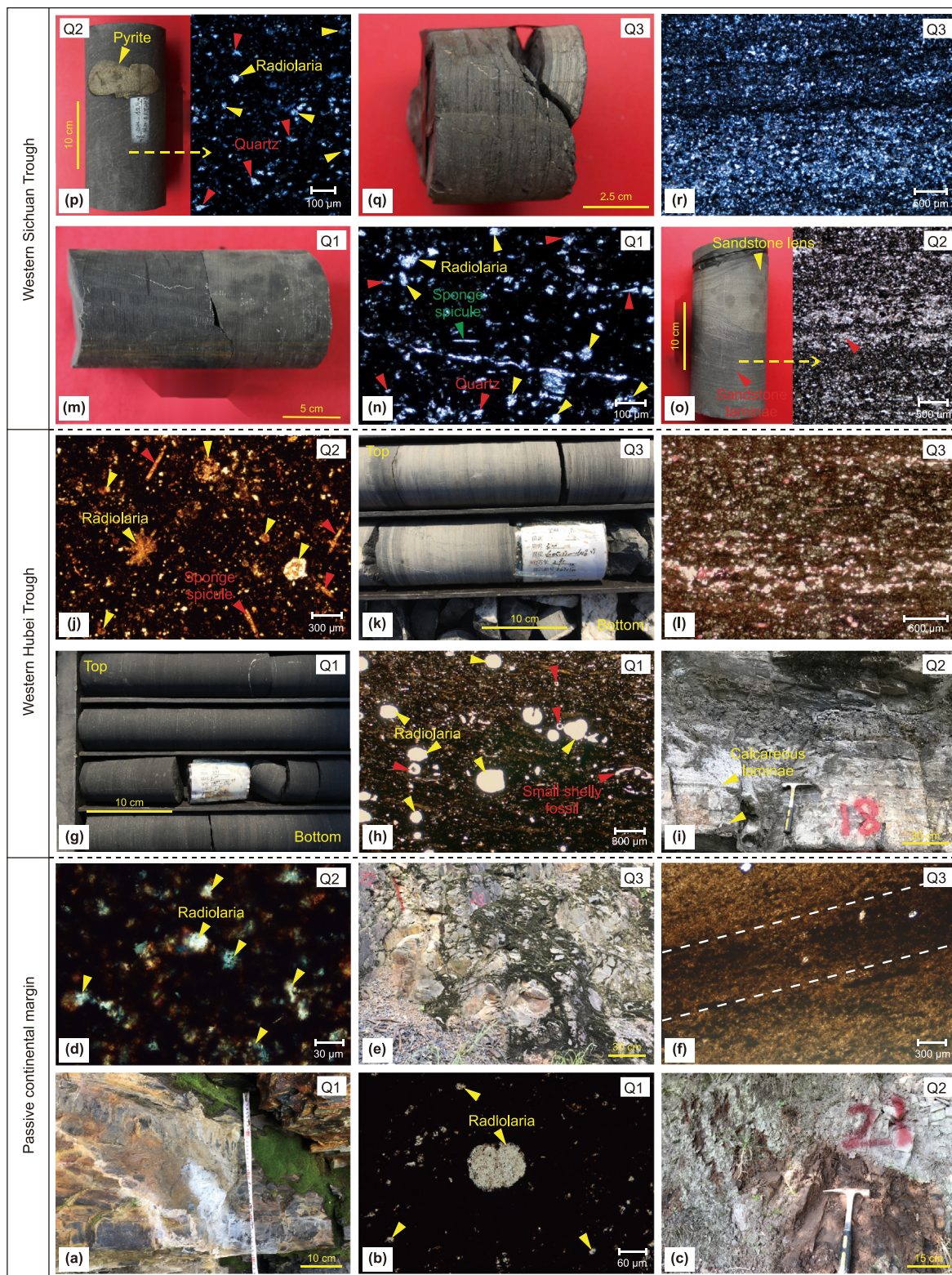
Fig. 4. Sedimentological and mineralogical petrological characteristics of the Qiongzhusi Formation in the study area. Passive continental margin area: **(a)** black siliceous rock, dominated by massive bedding, 14 layers, Q1, Morong; **(b)** siliceous rock with abundant siliceous radiolarians, 14 layers, Q1, Morong; **(c)** gray-black siliceous shale, dominated by massive bedding, 21 layers, Q2, Duodingguan; **(d)** siliceous shale with abundant siliceous radiolarians and siliceous bioclasts, 21 layers, Q2, Duodingguan; **(e)** dark gray silty shale, 23 layers, Q3, Duodingguan; **(f)** silty shale with fine-silty quartz particles are mainly dispersed in the clay-rich matrix, 23 layers, Q3, Duodingguan. Western Hubei Trough: **(g)** black siliceous shale, dominated by massive bedding, 1716.8−1717.8 m, Q1, YD2; **(h)** siliceous shale with abundant development of radiolarians (yellow arrow), visible small bivalve fossils (red arrow), 1717.6 m, Q1, YD2 well; **(i)** grayish-black calcareous siliceous mixed shale with extensive calcareous striated layers, 18 layers, Q2, Baizhuling; **(j)** calcareous siliceous mixed shale with incomplete calcite replacement of radiolarians (yellow arrows) and spicules (red arrows), 18 layers, Q2, Baizhuling; **(k)** gray calcareous shale, interbedded with dark gray clayey shale vein, 1748.2−1749.2 m, Q3, YD2; **(l)** calcareous shale with longitudinally interbedded calcareous and clay-rich layers of unequal thickness, 1748.5 m, Q3, YD2. Western Sichuan Trough: **(m)** gray-black carbonaceous shale, dominated by massive bedding, 2808.6 m, Q1, W201; **(n)** carbonaceous shale with visible subrounded biogenic silica

Al_2O_3 content (averages: 13.1% → 14.0% → 13.5% → 13.4%) and K/Al ratios (0.43 → 0.34 → 0.36 → 0.38) reflected an overall increase in the terrigenous input. However, in contrast to the passive continental margin and the western Hubei Trough, there was a significant decrease in the terrigenous input in the upper part of Q2 (still higher than that in Q1), which was closely related to the deep-water environment formed by the intensification of the regional rifting (which only occurred in the western Sichuan Trough area) (Liu et al., 2015, 2016). Furthermore, in the different depositional periods of the Qiongzhusi Formation, the feldspar content in the western Sichuan Trough area (from the paleo-continental felsic source area in western Sichuan) (Guo, 2023) and the carbonate rock content in the western Hubei Trough area were the highest in the entire area (Section 4.2). This indicates that these two areas were greatly affected by terrigenous sandy clasts and terrigenous carbonate clasts, respectively.

In conclusion, based on the comprehensive analysis of the proxy indices of the terrigenous input and the change trends of the rock and mineral characteristics, the above-mentioned changes in the terrigenous input that influenced the Qiongzhusi Formation in the study area were mainly controlled by the type of source area, sea level fluctuations, and the intensity of the extensional rifting activity.

5.2. Paleo-redox conditions

To accurately reflect the variations in the redox conditions of the water in which the shale in the Qiongzhusi Formation was deposited in the study area, proxy indicators such as the U/Th and Ni/Co ratios, the C-S-Fe-P system (C_{org}/P), and trace element enrichment coefficients (Mo_{EF} and U_{EF}) were studied (Jones and Manning, 1994; Algeo and Liu, 2020). In anaerobic environments, C_{org}/P is greater than 100, U/Th is greater than 1.25, and Ni/Co is greater than 7; whereas in oxygen-rich environments, C_{org}/P is less than 50, Ni/Co is less than 5, and U/Th is less than 0.75 (Wang et al., 2015). From the Q1 to Q3 depositional periods, the C_{org}/P, U/Th, Ni/Co, Mo_{EF}, and U_{EF} values in the passive continental margin exhibited overall gradual decreasing trends. The average changes were 223.9 → 212.0 → 38.1, 4.1 → 7.8 → 0.9, 24.9 → 9.7 → 3.7, 98.5 → 58.5 → 3.9, and 16.5 → 23.3 → 2.1, respectively. This indicates that the degree of bottom water reduction gradually weakened, and Q1 and Q2 were mainly anaerobic environments, while Q3 was mainly an oxygen-rich environment. The trends in the western Hubei Trough area were consistent with those in the passive continental margin (average changes of 298.4 → 80.8 → 52.4, 2.3 → 0.9 → 0.9, 7.3 → 4.2 → 4.3, 65.2 → 18.1 → 11.7, and 9.0 → 3.9 → 3.4, respectively), in that the bottom water environment changed from anaerobic to oxygen-depleted-oxygen-rich to oxygen-rich. After entering the western Sichuan Trough, the relevant parameters (the average changes from Q1 → lower middle part of Q2 → upper part of Q2 → Q3 were 81.4 → 29.5 → 47.1 → 28.6, 2.3 → 0.7 → 1.3 → 0.7, 6.0 → 3.2 → 4.2 → 3.5, 56.2 → 15.7 → 33.7 → 10.6, and 11.8 → 3.9 → 7.6 → 3.5, respectively) indicate that the bottom water environment changed from anaerobic-oxygen-poor to oxygen-enriched to oxygen-poor-oxygen-rich to oxygen-rich. The degree of bottom water reduction increased significantly in the upper part of Q2, which was different from the change in the western Hubei Trough and the western Sichuan Trough (Table 1, Fig. 5).

The above analysis shows that the degree of bottom water reduction in the Qiongzhusi Formation in the study area exhibited a significant weakening trend from bottom to top in both the passive continental margin and the western Hubei Trough area. However, the western Sichuan Trough exhibited oxidation in the upper part of Q2, which was closely related to the increase in the accommodation space caused by the intensification of the regional rifting.

In addition, the proxy indices of the organic-rich shale section at the bottom of the Qiongzhusi Formation (Q1) indicate that the passive continental margin had the strongest degree of bottom.

Water reduction, followed by the western Hubei Trough, and the western Sichuan Trough had the weakest degree of bottom water reduction.

5.3. Paleo-productivity levels

Elements in marine sediments such as Si, Ba, and P are the most widely used proxy indicators for the evaluation of paleo-productivity, and higher values indicate higher primary paleo-productivity levels. Since most sedimentary rocks contain both biogenic and terrigenous inputs, the levels of paleo-productivity are evaluated based on the content of the element fractions in the biogenic parts (Si_{XS} and Ba_{XS}) or the results of aluminum normalization (P/Al) after the removal of the terrigenous influence (Tribovillard et al., 2006; Algeo et al., 2011). It should be noted that sulfate reduction and iron oxide dissolution under anoxic conditions will lead to the decomposition of $BaSO_4$ and the release of P in organic matter, respectively, which distorts the Ba and P indicators (Tribovillard et al., 2006; Algeo et al., 2011; Rimmer, 2004). From Q1 to Q3, the Si_{XS} ($\times 10^{-4}$) (17.1 → 6.3 μg/g; Q3 missing), Ba_{XS} ($\times 10^{-2}$) (24.1 → 8.8 → 2.4 μg/g), and P/Al ($\times 104$) (128.7 → 51.7 → 38.9) values in the passive continental margin area all gradually decreased, indicating that the paleo-productivity gradually decreased. In the western Hubei Trough, the Si_{XS} ($\times 10^{-4}$) (13.2 → 4.4 → 3.7 μg/g) and Ba_{XS} ($\times 10^{-2}$) (16.5 → 7.4 → 5.0 μg/g) values also decreased, except for the higher Ba_{XS} value in the Q3 section due to weakening of the degree of reduction. The other values were lower than those in the passive continental margin during the same periods. However, P/Al (72.9 → 89.6 → 93.0) exhibited a diametrically inverse trend compared to the those of the Si_{XS} and Ba_{XS} values, and it is speculated that this increase was mainly related to the increased input of algae-rich (formed in water rich in N and P) (Zhang et al., 2015b) carbonate minerals (Wang et al., 2021; Liu et al., 2022b; Guo, 2023) from the central Hubei paleo-continent (where the Dengying Formation in the Sinian System forms the bedrock) (Liu et al., 2016) (Table 1, Figs. 2 and 5). Therefore, in this case, P/Al does not accurately indicate the changes in the paleo-productivity. Upon entering the western Sichuan Trough, the Si_{XS} ($\times 10^{-4}$) (7.2 → 6.9 → 6.4 → 7.9 μg/g), Ba_{XS} ($\times 10^{-2}$) (9.0 → 4.9 → 5.0 → 5.6 μg/g), and P/Al (146.2 → 158.6 → 189.7 → 190.6) values varied from Q1 to the lower middle part of Q2 to the upper part of Q2 to Q3. P/Al exhibited a longitudinally increasing trend, which was mainly controlled by the decrease in the degree of reduction (März et al., 2014). It has been pointed out that in areas where the bottom water is relatively reduced, the P content of sediments may not be high under high productivity conditions (such as the passive continental margin and the western Hubei Trough in the study area) (Ingall et al., 1993; Ingall and Jahnke, 1994; Kraal et al., 2010; Shen et al., 2015). Therefore, the P/Al values do not accurately indicate the change trends of the paleo-productivity in this region. The Ba_{XS} value

---

(yellow arrow) and subangular terrigenous silica (red arrow), 2808.6 m, Q1, W201; **(o)** gray silty shale with sandstone lens (yellow arrow) and sandy laminations development (red arrow), 2723.4 m, lower Q2, well W201; **(p)** gray-black carbonaceous shale with visible pyrite masses, microscopically visible subrounded biogenic silica (yellow arrows) and subangular terrigenous silica (red arrows), 2682.6 m, upper part of Q2, well W201; **(q)** gray argillaceous siltstone, 2632.0 m, Q3, well W201; **(r)** argillaceous siltstone with dark clayey laminations interbedded within bright sandy laminations, 2632.0 m, Q3, W201.
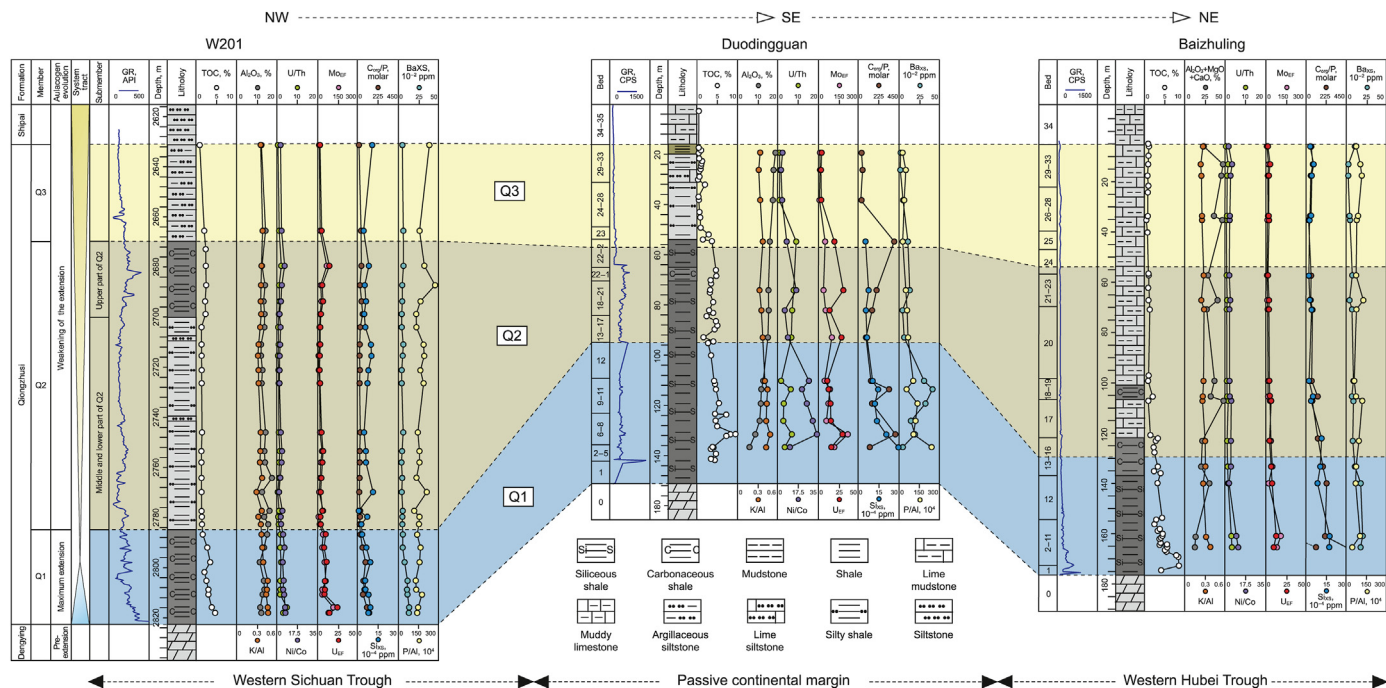
Fig. 5. Variations in the characteristics of the TOC content, terrigenous input (Al_2O_3, $Al_2O_3+MgO+CaO$, K/Al), paleo-redox conditions (U/Th, Ni/Co, Mo_{EF}, U_{EF}, and C_{org}/P), and paleo-productivity levels ($Si_{XS} \times 10^{-2}$, $Ba_{XS} \times 10^{-2}$, and $P/Al \times 10^4$) in the study area. The natural gamma data for the outcrops in Duodingguan and Baizhuling were measured using an HD-2000 handheld radiometer, and the test interval was 0.2−0.5 m.
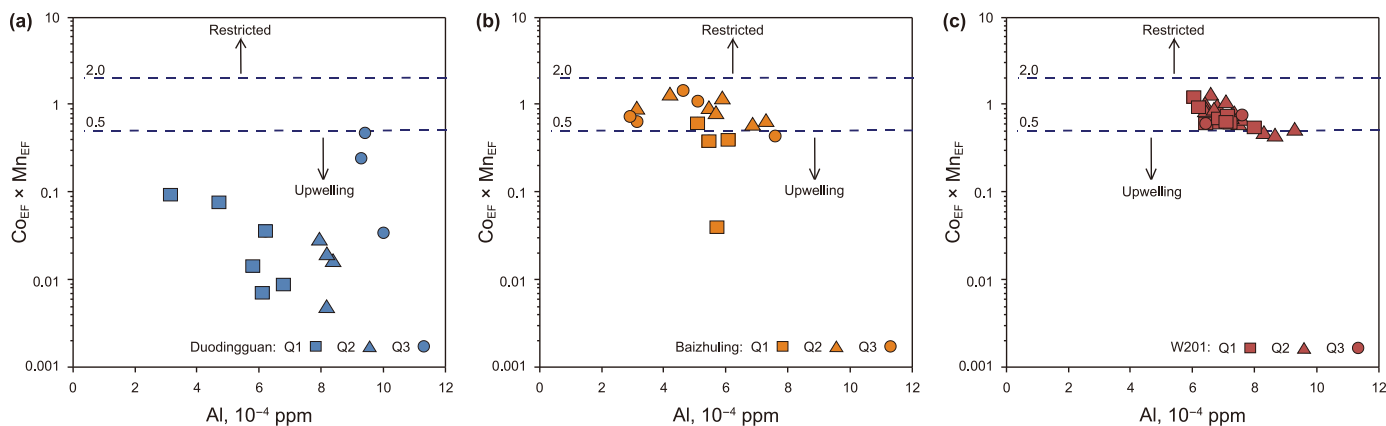

Fig. 6. Diagram showing the relationship between $Co_{EF} \times Mn_{EF}$ and Al during the depositional periods of the Qiongzhusi Formation in the study area: (**a**) passive continental margin, (**b**) western Hubei Trough, and (**c**) western Sichuan Trough (Sweere et al., 2016). The data points are from Table 1.
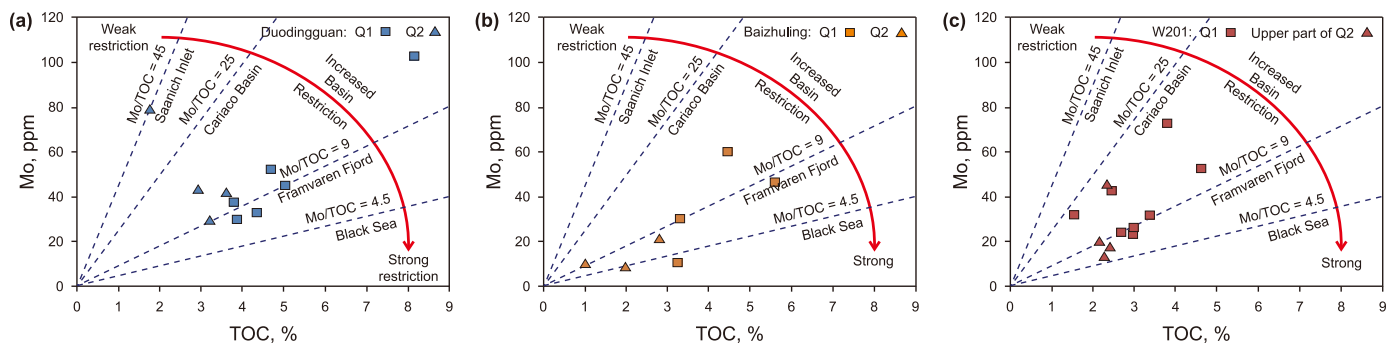
Fig. 7. Plot of the relationship between Mo and TOC during the depositional periods of the Qiongzhusi Formation: (**a**) passive continental margin, (**b**) western Hubei Trough, and (**c**) western Sichuan Trough. The data for the oxygen-rich environments have been excluded. The Mo/TOC values of the four modern ocean basins are from Tribovillard et al. (2006). The plotted data points are from Table 1.

exhibited a decreasing trend in the longitudinal direction, and the increase after the upper part of Q2 (below Q1) was mainly controlled by the decrease in the degree of reduction. The Ba_{XS} values in the horizontal direction were the lowest in the entire region during Q1 and Q2. Due to the significant influence of the terrigenous felsic clasts, the Si_{XS} value was a suitable indicator of the paleo-productivity levels in this area. For example, the Si_{XS} was the highest in the argillaceous siltstone in Q3.

The above analysis shows that the paleo-productivity levels of the Qiongzhusi Formation in the study area gradually decreased from bottom to top in both the passive continental margin and the western Hubei Trough areas. Although there was one period of increase in the western Sichuan Trough area after the deposition of the upper part of Q2, the overall trend was still a decreasing trend. In addition, during the main depositional period of the Qiongzhusi Formation shales, the paleo-productivity level was the highest in the passive continental margin, followed by the western Hubei Trough, and the western Sichuan Trough had the lowest paleo-productivity level.

5.4. Paleo-hydrological characteristics

Upwelling environments in continental margins (such as, the Peruvian Margin and Namibian Margin in the present ocean) are characterized by high primary productivity, mainly due to the large-scale transport of deep nutrient-rich seawater to the surface by upwelling currents. Nonetheless, the lack of resupply limits the enrichment of Co and Mn in sediments in the upwelling current zones due to the low contents of Co and Mn in deep seawater. However, in euxinic basins, Co and Mn are mainly input by rivers and are unlikely to develop to the point where their enrichment is

limited by insufficient supply. $Co_{EF} \times Mn_{EF}$ values of greater than 2 are associated with euxinic basins, those of less than 0.5 are associated with open/upwelling marine environments, and those between 0.5 and 2 are associated with environments that experience seasonal upwelling (Fig. 6) (Sweere et al., 2016). Ratios of redox-sensitive elements, e.g., Mo/TOC, are often used to determine the degree of seawater retention. Low Mo/TOC ratios indicate a strong water retaining environment, and vice versa (Fig. 7). However, this method is only suitable for anaerobic environments with certain water parameter constraints (Algeo and Lyons, 2006; Algeo and Rowe, 2012). In this study, the upwelling currents and water retention characteristics of the two sets of shale strata were compared and analyzed using the Al-$Co_{EF} \times Mn_{EF}$ and Mo/TOC plots, and the changes in their paleo-hydrological characteristics were investigated.

In the passive continental margin, the $Co_{EF} \times Mn_{EF}$ plots indicate that all of the depositional periods of the Qiongzhusi Formation were dominated by an open/upwelling environment. From Q1 to Q3, the $Co_{EF} \times Mn_{EF}$ values ($0.04 \rightarrow 0.02 \rightarrow 0.27$) exhibited an overall increasing trend, reflecting the weakening of the ocean current activity, while the Mo/TOC values ($9.6 \rightarrow 19.7$, not applicable to the oxygen-rich Q3) contradicted the hydrological properties (decreasing trend of the degree of retention) and were inconsistent with the geological background of sea level decline (Fig. 6(a) and 7(a), Table 1). This was mainly due to the fact that the open ocean environment of the passive continental margin had conditions conducive to the enrichment of both TOC and Mo. When both are enriched at the same time, the Mo/TOC value will be low, and the water holding capacity cannot be effectively determined (Xiao et al., 2019). In the western Hubei Trough, the $Co_{EF} \times Mn_{EF}$ plot indicates that the Q1 section was dominated by an open-seasonal
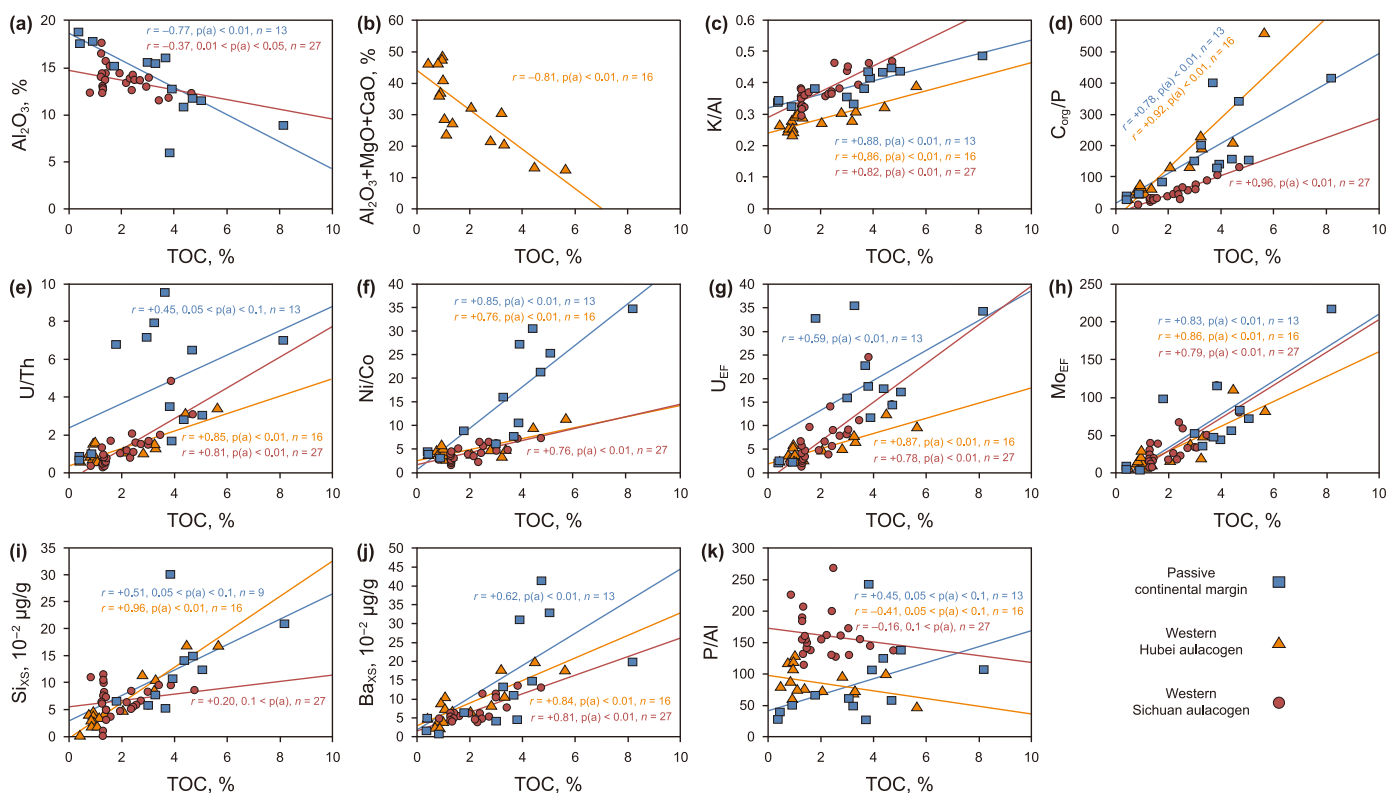

Fig. 8. The relationships between the TOC and the proxies of terrigenous input: **(a)** Al_2O_3, **(b)** $Al_2O_3 + MgO + CaO$, and **(c)** K/Al. The relationships between the TOC and the proxies of the paleo-redox conditions: **(d)** C_{org}/P, **(e)** U/Th, **(f)** Ni/Co, **(g)** U_{EF}, and **(h)** Mo_{EF}. The relationships between the TOC and the proxies of paleo-productivity: **(i)** $Si_{XS} \times 10^{-2}$, **(j)** $Ba_{XS} \times 10^{-2}$, and **(k)** (P/Al) $\times 10^4$. The data for the passive continental margin are from Duodingguan, the data for the western Hubei Trough are from Baizhuling, and the data for the western Sichuan Trough are from W201 (Table 1).
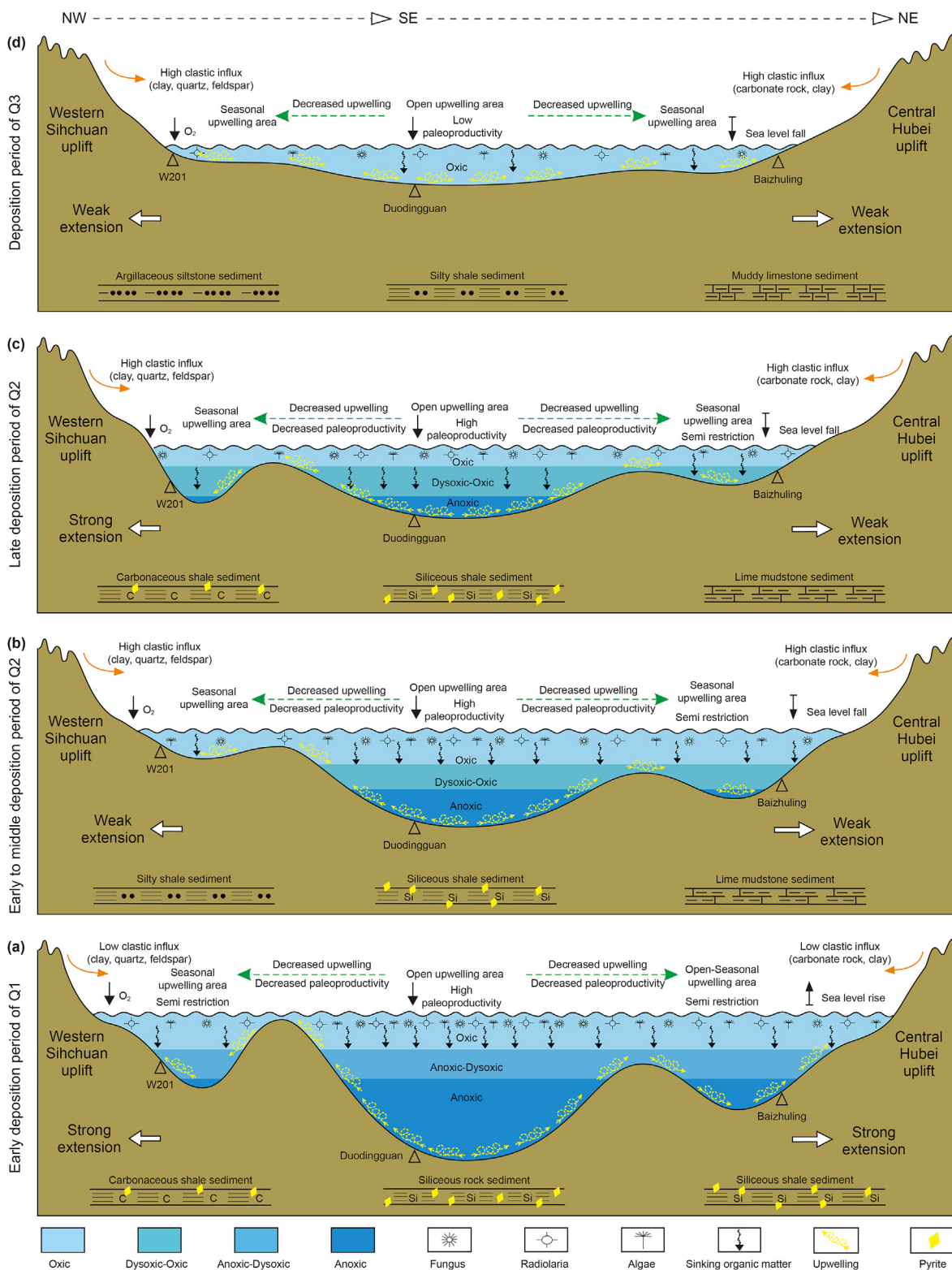
Fig. 9. Patterns of organic matter enrichment in different depositional periods for the Qiongzhusi Formation in the study area.

current transition environment and thereafter by a seasonal current, and the current activity was lower than that in the passive continental margin at different times. The $Co_{EF} \times Mn_{EF}$ values $(0.37 \rightarrow 0.92 \rightarrow 0.91)$ were not the same as the Mo/TOC values $(8.4 \rightarrow 7.1$, Q3 oxygen enriched), indicating that the paleo-

hydrological trends were consistent (Fig. 6(b) and 7(b), Table 1), the current activity weakened, and the degree of retention was enhanced. In the western Sichuan Trough, the $Co_{EF} \times Mn_{EF}$ values $(0.75 \rightarrow 0.72 \rightarrow 0.82 \rightarrow 0.66)$ indicate that the depositional periods of the Qiongzhusi Formation were dominated by seasonal ocean

currents, the current activity in different periods was lower than that in the passive continental margin, and the current activity during the Q1 period of high-quality shale sedimentation was lower than that of the western Hubei Trough.

The Mo/TOC ratio was 12.7 in Q1 and 10.1 in the upper part of Q2, indicating that the degree of retention increased and was significantly controlled by the sea level decline. Q2 and Q3 were deposited in oxygen-rich environments, and the Mo/TOC values were inapplicable as water holding capacity indicators (Fig. 6(c) and 7(c), Table 1).

Based on the above analysis, it was concluded that during the Q1 depositional period, the passive continental margin experienced the strongest ocean current activity due to its proximity to the ocean, the western Sichuan Trough experienced the weakest due to its distance from the passive continental margin and blockage by the Qianzhong Uplift (Tang, 2017), and the current activity (somewhat between that in both regions) in the western Hubei Trough was weakest due to its proximity to the passive continental margin. During the Q2→Q3 depositional periods, the water holding capacity increased as the sea level fell, the ocean current activity decreased in the passive continental margin and western Hubei Trough, and the current activity in the western Sichuan Trough did not obviously change. This is speculated to be related to the fact that the current activity in the western Sichuan Trough has always been at a low level.

5.5. Main factors controlling organic matter enrichment

As can be seen from Fig. 8, the TOC content as negatively correlated with the Al_2O_3 (or $Al_2O_3+MgO + CaO$) content across the entire study area, but was positively correlated with K/Al, C_{org}/P, U/Th, Ni/Co, U_{EF}, Mo_{EF}, and Ba_{XS}. In the passive continental margin and the western Hubei Trough, the TOC content was positively correlated with Si_{XS}, while the correlation between the TOC content and Si_{XS} in the western Sichuan Trough was poor due to the significant influence of terrigenous felsic clasts. Moreover, the application of the parameter Si_{XS} in this area has limitations. The P/Al ratio was only positively correlated with the TOC content in the passive continental margin area, and it was negatively correlated with the TOC content in the western Hubei Trough and the west Sichuan Trough. These correlations were related to the increased input of carbonate clasts and the decreased reduction of carbonate clasts in the Dengying Formation, respectively. This in turn affected the enrichment of P, rendering the parameter P/Al unsuitable as a paleo-productivity indicator. Based on the above analysis, the redox conditions, paleo-productivity levels, and terrigenous input all affected the organic matter enrichment in the study area.

(1) Q1 depositional period

During the Q1 depositional period (Fig. 9(a)), the Yangtze region was located in the tropical-subtropical climate belt near the equator, coinciding with a significant global sea level rise. This period was characterized by deepwater sedimentary conditions (Xiao et al., 2021). Simultaneously, intense fracturing occurred in the shallow crustal layer of the Yangtze region due to the downward force exerted by plate subduction in the original Tethys Ocean. This led to heightened tectonic basin activity within the area, resulting in an increased capacity for accommodation (Liu et al., 2016, 2017; Wu et al., 2020a). All of the shallow carbonate platforms developed in the early stage of the Yangtze Plate were inundated by seawater (Liu et al., 2016), and overall, the study area had an uncompensated anoxic water environment. Meanwhile, Rocky Mountains Burgess Shale and Spence Shale in Utah, North American are also found in anoxic environments (Gaines et al.,

2012; Garson et al., 2012). The passive continental margin area was close to the ocean, far from the paleocontinent, weakly affected by terrigenous sources, and in an open current environment, so it was capable of carrying large quantities of the nutrients (such as Si, Ba, and P) required for biological activities into the Yangtze Basin from the deep ocean, providing a basis for the plentiful occurrence of the subsequently fossilized bivalves, radiolarians, and fungal organisms (Wu et al., 2020a). The high level of paleo-productivity, favorable preservation conditions, and low terrigenous input in the passive continental margin area were conducive to large-scale organic matter enrichment dominated by organic-rich biogenic siliceous sediments, and the TOC content was the highest for the entire region. Compared with the passive continental margin, the depositional water became shallower, the input of terrigenous carbonate clasts was relatively high, the degree of bottom water reduction was lower, the water holding capacity increased, the ocean current activity weakened, the level of paleo-productivity decreased, and the TOC content decreased. The western Sichuan Trough was far from the ocean and close to the western Sichuan paleocontinent (Tang, 2017). Upon entering the western Sichuan Trough, the depositional water body was relatively shallow, the degree of bottom water reduction (anaerobic-poor oxygen) was the weakest in the entire region, and the input of terrigenous felsic clasts (western Sichuan paleocontinent) was relatively large (feldspar content was the highest in the entire region), due to the isolation by the Qianzhong Uplift (Tang, 2017). The upwelling activity was the weakest in the entire region, the interconnectivity with the seawater from the deep ocean was poor, and the level of paleo-productivity was the lowest, resulting in the lowest TOC content in the entire region. Carbonaceous shale (both biogenic silica and terrigenous silica) sedimentation was dominant. During this period, the change in the intensity of the ocean current activity (which caused the change in the paleo-productivity) was the main factor controlling the differences in the organic matter enrichment across the different regions.

(2) Q2 depositional period

During the Q2 depositional period (Fig. 9(b) and (c)), the global oceans entered a gradual process of oxidation (Li et al., 2020). The overall rifting weakened from the rift extensional stage to the infilling stage (Liu et al., 2015, 2016), the sea level continued to fall, and the sedimentary pattern in the Yangtze region did not change significantly compared with the Q1 period (Liu et al., 2016; Xie, 2021). However, the accommodation space in the area decreased by varying degrees. The passive continental margin area still maintained a relatively high sea level, and the bottom water environment was predominantly anaerobic. The area was well-connected with the ocean as it was still an open current environment and had the strongest ocean current activity in the entire region. In addition, the paleo-productivity was also the highest of the entire region. The drop of sea level during this period had two main effects on the organic matter enrichment: 1) it decreased the degree of reduction of the bottom water and worsened the preservation conditions of the organic matter, and 2) the terrigenous input increased, which had a diluting effect on the organic matter (Lu et al., 2019). As a result, the TOC content decreased significantly compared with that in Q1, which was dominated by interbedded biogenic siliceous rocks and siliceous shale. The depositional water was significantly shallower in the western Hubei Trough than in the passive continental, which was due to the increased input of carbonate rock clasts in the central Hubei region and the increased oxygen content of the bottom water. During this period the environments were predominantly oxygen-poor or oxygen-rich, which led to distinctly poor storage conditions. In addition, the ocean

current activity was also significantly weaker than in the passive continental margin, resulting in a significant decrease in the level of paleo-productivity. The TOC content of the shales was significantly reduced due to the above-mentioned paleoenvironmental changes, and they mainly consisted of a mixture of clay, siliceous, and calcareous shale deposits. According to the changes in the tectonic activity, the sedimentation can be divided into two stages after entering the western Sichuan Trough. 1) In the early to middle stages of Q2 (Fig. 9(b)), the extensional rifting activity was weak, the sea level was low, the accommodation space was small, the conditions for organic matter enrichment were significantly worse than those in the passive continental margin, the TOC content was low, and silty shale was mainly deposited. 2) In the late stages of Q2 (Fig. 9(c)), the sea level continued to fall and the regional rifting intensified again (only in the western Sichuan Trough area) (Liu et al., 2016), resulting in a significant increase in the accommodation space. However, the conditions for organic matter enrichment improved, and the TOC content was still lower than that in the passive continental margin, which was dominated by the deposition of carbonaceous shale. During this period, the preservation conditions, ocean current activities, and terrigenous input all exerted clear controls on the organic matter enrichment in the area.

(3) Q3 depositional period

During the Q3 depositional period (Fig. 9(d)), the sea level in the study area further decreased, the rifting continued to weaken (Liu et al., 2016), the accommodation space continued to decrease, the study area as a whole was in an oxygen-rich environment, and the terrigenous input increased. The uplift and depression pattern in the Yangtze region gradually disappeared (Liu et al., 2016; Xiao et al., 2021), the TOC content was the lowest, and there was no significant difference across the different zones. During this period, the preservation conditions were the main factors controlling the organic matter enrichment.

6. Conclusions

(1) Longitudinally, the TOC content gradually decreased from bottom to top, and the distribution of the high-quality shale in the different zones exhibited certain differences: the organic-rich shale (TOC > 2%) in the passive continental margin area was mainly distributed throughout Q1 and Q2. In the western Hubei Trough area, this shale was mainly distributed throughout Q1, and in the western Sichuan Trough area, it was mainly distributed throughout the upper parts of Q1 and Q2. Latitudinally, the TOC content exhibited the same decreasing trend from the passive continental margin to the craton depression. The western Hubei Trough area had a greater TOC content than the western Sichuan Trough area during the Q1 period. It was lower than the western Sichuan Trough area by the end of Q2, and there was no significant difference in the other periods.

(2) During the Q1 period, the passive continental margin was dominated by biogenic siliceous sediments. The carbonate rock and feldspar contents increased significantly, while the biogenic silica content decreased significantly from this area to the western Hubei Trough or the western Sichuan Trough, and there was a lithofacies transition to biogenic siliceous or carbonaceous shale. During the Q2 period, the passive continental margin was dominated by biological siliceous shale. There was a lithofacies transition to clayey, calcareous, and siliceous mixed shales towards the western Hubei Trough, and there was a lithofacies transition to silty shale (early-middle part of Q2) and carbonaceous shale (end of Q2)

towards the western Sichuan Trough. During the Q3 period, the Yangtze platform entered a period of infilling, and the passive continental margin area was dominated by the deposition of silty shale, the western Hubei Trough was dominated by argillaceous limestone, and the western Sichuan Trough was dominated by argillaceous siltstone.

(3) During the Q1 period, there was a high sea level, rifting was strong, and the entire area was characterized by a low terrigenous input and bottom water hypoxia. Sea level rise was the main factor controlling the differences in the organic matter enrichment: from the passive continental margin to the western Hubei Trough to the western Sichuan Trough, the ocean current activity gradually weakened, the paleo-productivity decreased, and the TOC content decreased. During the Q2 period, the rifting began to weaken, the sea level decreased, and ocean currents, preservation conditions, and terrigenous input all exerted clear controlling effects on the organic matter enrichment in the area. From the passive continental margin to the craton depression, the organic matter enrichment conditions deteriorated and the TOC content decreased significantly. It should be noted that the local intensification of the rifting in the western Sichuan Trough at the end of Q2 improved the conditions for organic matter enrichment, and the TOC content briefly increased. During the Q3 period, the sea level continued to fall and the rifting weakened further. As a whole, the study area became an oxygen-rich environment, and the preservation conditions became the main factor controlling the organic matter enrichment. The TOC content was low overall, and the differences across the different zones were not apparent.

CRediT authorship contribution statement

Cheng-Lin Ye: Writing – original draft. **Jun–Jun Shen:** Writing – review & editing. **Shan-Shan Li:** Formal analysis. **Yu-Man Wang:** Methodology. **Guang-Chao Tan:** Data curation. **Jia-Kai Yan:** Investigation. **Lin Zhou:** Resources. **Ji-Yong Liu:** Resources.

Declaration of competing interest

We declare that we have no financial and personal relationships with other people or organizations that can inappropriately influence our work, there is no professional or other personal interest of any nature or kind in any product, service and/or company that could be construed as influencing the position in, or the review of, the manuscript entitled.

Acknowledgements

References

Algeo, T.J., Liu, J.S., 2020. A re-assessment of elemental proxies for paleoredox analysis. Chem. Geol. 540, 119549. https://doi.org/10.1016/j.chemgeo.2020.119549.

Algeo, T.J., Lyons, T.W., 2006. Mo–total organic carbon covariation in modern anoxic marine environments: implications for analysis of paleoredox and paleohydrographic conditions. Paleoceanography 21, 1–23. https://doi.org/10.1029/2004PA001112.

Algeo, T.J., Rowe, H., 2012. Paleoceanographic applications of trace-metal concentration data. Chem. Geol. 324, 6–18. https://doi.org/10.1016/j.chemgeo.2011.09.002.

Algeo, T.J., Kuwahara, K., Sano, H., Bates, S., Lyons, T., Elswick, E., Hinnov, L.,

Ellwood, B., Moser, J., Maynard, J.B., 2011. Spatial variation in sediment fluxes, redox conditions, and productivity in the Permian-Triassic Panthalassic Ocean. Palaeogeogr. Palaeoclimatol. Palaeoecol. 308, 65—83. https://doi.org/10.1016/j.palaeo.2010.07.007.

Awan, R.S., Liu, C.L., Gong, H.W., Dun, C., Tong, C., 2020. Chamssidini, LG. Paleosedimentary environment in relation to enrichment of organic matter of Early Cambrian black rocks of Niutitang Formation from Xiangxi area China. Mar. Petrol. Geol. 112, 1—20. https://doi.org/10.1016/j.marpetgeo.2019.104057.

Canfield, D.E., Poulton, S.W., Knoll, A.H., Narbonne, G.M., Ross, G., Goldberg, T., Strauss, H., 2008. Ferruginous conditions dominated Later Neoproterozoic deep-water chemistry. Science 321, 949—952. https://doi.org/10.1126/science.1154499.

Chang, H.J., Chu, X.L., Feng, L.J., 2018. Marine redox stratification on the earliest Cambrian (ca. 542—529 Ma) Yangtze platform. Palaeogeogr. Palaeoclimatol. Palaeoecol. 504, 75—85. https://doi.org/10.1016/j.palaeo.2018.05.007.

Erwin, D.H., Laflamme, M., Tweedt, S.M., Sperling, E.A., Pisani, D., Peterson, K.J., 2011. The Cambrian conundrum: early divergence and later ecological success in the early history of animals. Science 334, 1091—1097. https://doi.org/10.1126/science.1206375.

Fan, H.J., Deng, H.C., Fu, M.Y., Liu, S.B., Yu, H.Z., Li, Y.L., 2021. Sedimentary characteristics of the lower cambrian Qiongzhusi Formation in the Sichuan Basin and its response to construction. Acta Sedimentol. Sin. 39, 1004—1019. https://doi.org/10.14027/j.issn.1000-0550.2020.041 (in Chinese).

Fang, X.Y., Wu, L.L., Geng, A.S., Deng, Q., 2019. Formation and evolution of the ediacaran to lower cambrian black shales in the Yangtze platform, South China. Palaeogeogr. Palaeoclimatol. Palaeoecol. 527, 87—102. https://doi.org/10.1016/j.palaeo.2019.04.025.

Gaines, R.R., Hammarlund, E.U., Hou, X., Qi, C., Gabbott, S.E., Zhao, Y., Peng, J., Canfield, D.E., 2012. The Mechanism of Burgess Shale-type Preservation, vol. 109. Proceedings of the National Academy of Sciences, pp. 5180—5184. https://doi.org/10.1073/pnas.1111784109.

Gao, P., He, Z., Li, S., Lash, G.G., Li, B., Huang, B., Yan, D., 2018. Volcanic and hydrothermal activities recorded in phosphate nodules from the Lower Cambrian Niutitang Formation black shales in South China. Palaeogeogr. Palaeoclimatol. Palaeoecol. 505, 381—397. https://doi.org/10.1016/j.palaeo.2018.06.019.

Garson, D.E., Gaines, R.R., Droser, M.L., Liddell, W.D., Sappenfield, A., 2012. Dynamic palaeoredox and exceptional preservation in the cambrian spence shale of Utah. Lethaia 45, 164—177. https://doi.org/10.1111/j.1502-3931.2011.00266.x.

Goldberg, T., Strauss, H., Guo, Q., Liu, C., 2007. Reconstructing marine redox conditions for the Early Cambrian Yangtze Platform: evidence from biogenic sulphur and organic carbon isotopes. Palaeogeogr. Palaeoclimatol. Palaeoecol. 254, 175—193. https://doi.org/10.1016/j.palaeo.2007.03.015.

Gu, H., Wang, J., Wei, H.Y., Fu, X.G., 2022. Controlling factors of organic enrichment in the Shuijingtuo Formation in the lower cambrian of the Chengkou area, Sichuan Basin. Acta Sedimentol. Sin. 1—25. https://doi.org/10.14027/j.issn.1000-0550.2022.091 (in Chinese).

Guo, S., 2023. Refined Classification of the Material Composition of the Early Cambrain Black Shale in Guizhou and its Control on Reservoir Physical Properties. China University of Mining and Technology, pp. 28—30. https://doi.org/10.27623/d.cnki.gzkyu.2023.000151 (in Chinese).

He, Q., Gao, J., Dong, T., He, S., Zhai, G.Y., Zou, G.F., 2021. Elemental geochemistry and paleo-environmental conditions of the lower cambrian Niutitang shale in western Hubei Province. Acta Sedimentol. Sin. 39, 686—703. https://doi.org/10.14027/j.issn.1000-0550.2020.107 (in Chinese).

Hoffman, P.F., Li, Z.X., 2009. A palaeogeographic context for Neoproterozoic glaciation. Palaeogeogr. Palaeoclimatol. Palaeoecol. 277, 158—172. https://doi.org/10.1016/j.palaeo.2009.03.013.

Ingall, E., Jahnke, R., 1994. Evidence for enhanced phosphorus regeneration from marine sediments overlain by oxygen depleted waters. Geochem. Cosmochim. Acta 58, 2571—2575. https://doi.org/10.1016/0016-7037(94)90033-7.

Ingall, E.D., Bustin, R.M., Cappellen, P.V., 1993. Influence of water column anoxia on the burial and preservation of carbon and phosphorus in marine shales. Geochem. Cosmochim. Acta 57, 303—316. https://doi.org/10.1016/S0025-3227(96)00112-0.

Jin, C.S., Li, C., Algeo, T.J., Planavsky, N.J., Cui, H., Yang, X., Zhao, Y., Zhang, X., Xie, S., 2016. A highly redox-heterogeneous ocean in South China during the early Cambrian (~529—514 Ma): implications for biota-environment co-evolution. Earth Planet Sci. Lett. 441, 38—51. https://doi.org/10.1016/j.epsl.2016.02.019.

Jin, C.S., Li, C., Algeo, T.J., Wu, S.Y., Cheng, M., Zhang, Z.H., Shi, W., 2020. Controls on organic matter accumulation on the early-Cambrian western Yangtze Platform, South China. Mar. Petrol. Geol. 111, 75—87. https://doi.org/10.1016/j.marpetgeo.2019.08.005.

Jones, B., Manning, D.A.C., 1994. Comparison of geochemical indices used for the interpretation of palaeoredox conditions in ancient mudstone. Chem. Geol. 111, 111—129. https://doi.org/10.1016/0009-2541(94)90085-X.

Kraal, P., Slomp, C.P., Forster, A., Kuypers, M.M.M., 2010. Phosphorus cycling from the margin to abyssal depths in the proto-Atlantic during oceanic anoxic event. Palaeogeogr. Palaeoclimatol. Palaeoecol. 295, 42—54. https://doi.org/10.1016/j.palaeo.2010.05.014.

Laflamme, M., Darroch, S.A., Tweedt, S.M., Peterson, K.J., Erwin, D.H., 2013. The end of the Ediacara biota: extinction, biotic replacement, or Cheshire Cat? Gondwana Res. 23, 558—573. https://doi.org/10.1016/j.gr.2012.11.004.

Li, Z.X., Bogdanova, S., Collins, A., Davidson, A., De Waele, B., Ernst, R., Fitzsimons, I., Fuck, R., Gladkochub, D., Jacobs, J., 2008. Assembly, configuration, and break-up history of Rodinia: a synthesis. Precambrian Res. 160, 179—210. https://doi.org/10.1016/j.precamres.2007.04.021.

Li, C., Shi, W., Cheng, M., Jin, C.S., Algeo, T.J., 2020. The redox structure of Ediacaran and early Cambrian oceans and its controls. Sci. Bull. 65, 2141—2149. https://doi.org/10.1016/j.scib.2020.09.023.

Liu, S.G., Sun, W., Song, J.M., Deng, B., Zhong, Y., Luo, C., Ran, B., Tian, H.Y., Li, Z.B., Peng, H.L., Yin, K.W., 2015. Tectonics-controlled distribution of marine petroleum accumulations in the Sichuan Basin, China. Earth Sci. Front. 22, 146—160. https://doi.org/10.13745/j.esf.2015.03.013 (in Chinese).

Liu, S.G., Wang, Y.G., Sun, W., Zhong, Y., Hong, H.T., Deng, B., Xia, M.L., Song, J.M., Wen, Y.C., Wu, J., 2016. Control of intracratonic sags on the hydrocarbon accumulations in the marine strata across the Sichuan Basin, China. Journal of Chengdu University of Technology 43, 1—23. https://doi.org/10.3969/j.issn.1671-9727.2016.01.01 (in Chinese).

Liu, Z.B., Gao, B., Zhang, Y.Y., Du, W., Nie, H.K., 2017. Types and distribution of the shale sedimentary facies of the lower cambrian in upper Yangtze area, South China. Petrol. Explor. Dev. 44, 21—31. https://doi.org/10.1016/S1876-3804(17)30004-6.

Liu, Z.X., Yan, D.T., Yuan, D.E., Niu, X., Fu, H.J., 2022a. Multiple controls on the organic matter accumulation in early Cambrian marine black shales, middle Yangtze Block, South China. J. Nat. Gas Sci. Eng. 100, 104454. https://doi.org/10.1016/j.jngse.2022.104454.

Liu, Z.B., Wang, P.W., Nie, H.K., Li, P., Li, Q.W., 2022b. Enrichment conditions and favorable prospecting targets of Cambrian shale gas in Middle-Upper Yangtze. J. Cent. S. Univ. 53, 3694—3707. https://doi.org/10.11817/j.issn.1672-7207.2022.09.031 (in Chinese).

Lu, Y.B., Jiang, S., Lu, Y.C., Xu, S., Shu, Yi, Wang, Y.X., 2019. Productivity or preservation? The factors controlling the organic matter accumulation in the late Katian through Hirnantian Wufeng organic-rich shale, South China. Mar. Petrol. Geol. 109, 22—35. https://doi.org/10.1016/j.marpetgeo.2019.06.007.

Ma, Y.S., Chen, H.D., Wang, G.L., 2009. Tectonic Sequence Stratigraphy and Lithofacies Paleogeography of Sinian-Neogene in Southern China. Chinese Science Publishing Company, Beijing, China, pp. 60—65.

Ma, Y.Q., Lu, Y.C., Liu, X.F., Zhai, G.Y., Wang, Y.F., Zhang, C., 2019. Depositional environment and organic matter enrichment of the lower Cambrian Niutitang shale in western Hubei Province, South China. Mar. Petrol. Geol. 109, 381—393. https://doi.org/10.1016/j.marpetgeo.2019.06.039.

März, C., Poulton, S.W., Wagner, T., Schnetger, B., Brumsack, H.J., 2014. Phosphorus burial and diagenesis in the central bering sea (Bowers ridge, IODP site U1341): perspectives on the marine P cycle. Chem. Geol. 363, 270—282. https://doi.org/10.1016/j.chemgeo.2013.11.004.

Murphy, A.E., Sageman, B.B., Hollander, D.J., Lyons, T.W., Brett, C.E., 2000. Black shale deposition and faunal overturn in the Devonian Appalachian Basin: clastic starvation, seasonal water-column mixing, and efficient biolimiting nutrient recycling. Paleoceanography 15, 280—291. https://doi.org/10.1029/1999PA000445.

Murray, R.W., Leinen, M., 1996. Scavenged excess aluminum and its relationship to bulk titanium in biogenic sediment from the central equatorial Pacific Ocean. Geochem. Cosmochim. Acta 60, 3869—3878. https://doi.org/10.1016/0016-7037(96)00236-0.

Pedersen, T.F., Calvert, S.E., 1990. Anoxia vs productivity: what controls the formation of organic—carbon—rich sediments and sedimentary rocks? AAPG Bull. 74, 454—466. https://doi.org/10.1306/0C9B232B-1710-11D7-8645000102C1865D.

Qiu, Z., Zou, C.N., Mills, B.J.W., Xiong, Y.J., Tao, H.F., Lu, H.L., Xiao, W.J., Poulton, S.W., 2022. A nutrient control on expanded anoxia and global cooling during the Late Ordovician mass extinction. Communications Earth & Environment 3, 82. https://doi.org/10.1038/s43247-022-00412-x.

Rimmer, S.M., 2004. Geochemical paleoredox indicators in devonian—mississippian black shales, central appalachian basin (USA). Chem. Geol. 206, 373—391. https://doi.org/10.1016/j.chemgeo.2003.12.029.

Shen, J., Schoepfer, S.D., Feng, Q.L., Zhou, L., Yu, J.X., Song, H.Y., Wei, H.Y., Algeo, T.J., 2015. Marine productivity changes during the end-Permian crisis and Early Triassic recovery. Earth Sci. Rev. 149, 136—162. https://doi.org/10.1016/j.earscirev.2014.11.002.

Sweere, T., Boorn, S., Dickson, A.J., Reichart, G., 2016. Definition of new trace-metal proxies for the controls on organic matter enrichment in marine sediments based on Mn, Co, Mo and Cd concentrations. Chem. Geol. 441, 235—245. https://doi.org/10.1016/j.chemgeo.2016.08.028.

Tang, L., 2017. Study on Lithofacies Paleogeography of Lower Cambrian in Sichuan Basin. Yangtze University, pp. 41—45. https://doi.org/10.26986/d.cnki.gcdlc.2019.001133 (in Chinese).

Tribovillard, N., Algeo, T.J., Lyons, T., Riboulleau, A., 2006. Trace metals as paleoredox and paleoproductivity proxies: an update. Chem. Geol. 232, 12—32. https://doi.org/10.1016/j.chemgeo.2006.02.012.

Wang, S.F., Zou, C.N., Dong, D.Z., Wang, Y.M., Li, X.J., Huang, J.L., Guan, Q.Z., 2015. Multiple controls on the paleoenvironment of the Early Cambrian marine black shales in the Sichuan Basin, SW China: geochemical and organic carbon isotopic evidence. Mar. Petrol. Geol. 66, 660—672. https://doi.org/10.1016/j.marpetgeo.2021.105434.

Wang, N., Li, M.J., Tian, X.W., Hong, H.T., 2019. Main factors controlling the OM enrichment in the lower cambrian sediments of the Sichuan Basin, SW China. Geol. J. 55, 3083—3096. https://doi.org/10.1002/gj.3581.

Wang, N., Li, M.J., Tian, X.W., Hong, H.T., Wen, L., Wang, W.Z., 2020. Climate-ocean control on the depositional watermass conditions and organic matter enrichment in Lower Cambrian black shale in the upper Yangtze Platform. Mar. Petrol.

Geol. 120, 104570. https://doi.org/10.1016/j.marpetgeo.2020.104570.

Wang, Y.M., Shen, J.J., Qiu, Z., Li, X.J., Zhang, L.F., Zhang, Q., Wang, C.H., 2021. Characteristics and environmental significance of concretion in the lower cambrian Qiongzhusi Formation in the middle-upper Yangtze area. Nat. Gas Geosci. 32, 1308–1323. https://doi.org/10.1016/j.jnggs.2021.12.004 (in Chinese).

Wu, S.Q., Guo, J.H., Wang, X.K., Li, Z.Y., Liu, C.S., Jiao, P., 2020a. Geochemical characteristics and organic matter enrichment mechanism of the Lower Cambrian Niutitang formation black rock series in central Hunan. J. Cent. S. Univ. 51, 2049–2060. https://doi.org/10.11817/j.issn.1672-7207.2020.08.001 (in Chinese).

Wu, Y.W., Tian, H., Gong, D.J., Li, T.F., Zhou, Q., 2020b. Paleo-environmental variation and its control on organic matter enrichment of black shales from shallow shelf to slope regions on the Upper Yangtze Platform during Cambrian Stage 3. Palaeogeogr. Palaeoclimatol. Palaeoecol. 545, 1–20. https://doi.org/10.1016/j.palaeo.2020.109653.

Xia, W., Yu, B.S., Wang, Y.H., Sun, M.D., 2017. Study on the depositional environment and organic accumulation mechanism in the niutitang and longmaxi formation, North Guizhou Province: a case study of well Renye1 and well Xiye1. J. Mineral. Petrol. 37, 77–89. https://doi.org/10.19719/j.cnki.1001-6872.2017.03.011 (in Chinese).

Xia, P., Fu, Y., Yang, Z., Guo, C., Huang, J.Q., Huang, M.Y., 2020. The relationship between sedimentary environment and organic matter accumulation in the Niutitang black shale in Zhenyuan, Northern Guizhou. Acta Geol. Sin. 94, 947–956. https://doi.org/10.3724/SP.J.0001-571720200301 (in Chinese).

Xiang, L, Schoepfer, S.D., Zhang, H., Cao, C.Q., Shen, S.Z., 2018. Evolution of primary producers and productivity across the Ediacaran-Cambrian transition. Precambrian Res. 313, 68–77. https://doi.org/10.1016/j.precamres.2018.05.023.

Xiao, B., Liu, S.G., Ran, B., Yang, D., Han, Y.Y., 2019. Identification of organic matter enrichment factors in marine sedimentary rocks based on elements Mn, Co, Cd and Mo: application in the northern margin of Sichuan Basin, South China. Geol. Rev. 65, 1316–1330. https://doi.org/10.16509/j.georeview.2019.06.002 (in Chinese).

Xiao, B., Liu, S.G., Ran, B., Li, Z.B., Ye, Y.H., Han, Y.Y., 2021. Study on sedimentary tectonic pattern of wufeng Formation and Longmaxi Formation in the northern margin of Sichuan Basin, South China. Earth Science 46, 2449–2465. https://doi.org/10.3799/dqkx.2020.208 (in Chinese).

Xie, H.G., 2021. Characteristics and research progress of geological structure of Western Hubei trough. Journal of Jianghan Petroleum University of Staff and Workers 34, 10–13. https://doi.org/10.3969/j.issn.1009-301X.2021.02.004 (in Chinese).

Yeasmin, R., Chen, D.Z., Fu, Y., Wang, J., Guo, Z., Guo, C., 2017. Climatic-oceanic forcing on the organic accumulation across the shelf during the early cambrian (Age 2 through 3) in the mid-upper Yangtze block, NE Guizhou, South China. J. Asian Earth Sci. 134, 365–386. https://doi.org/10.1016/j.jseaes.2016.08.019.

Zhang, S.C., Zhang, B.M., Bian, L.Z., Jin, Z.J., Wang, D.Y., Zhang, X.Y., Gao, Z.Y., Chen, J.F., 2005. Development constraints of marine source rocks in China. Earth Sci. Front. 12, 39–48 (in Chinese).

Zhang, S., Li, H., Jiang, G., Evans, D.A.D., Dong, J., Wu, H., Yang, T., Liu, P., Xiao, Q., 2015a. New paleomagnetic results from the Ediacaran Doushantuo Formation in South China and their paleogeographic implications. Precambrian Res. 259, 130–142. https://doi.org/10.1016/j.precamres.2014.09.018.

Zhang, W., Yang, R.D., Mao, T., Reng, H.L., Gao, J.B., Chen, J.Y., 2015b. Sedimentary environment and mineralization mechanism of the stromatolitic phosphorite in the ediacaran Dengying Formation, Wengan county of Guizhou Province. China. Geol. J. China Univ. 21, 186–195. https://doi.org/10.16108/j.issn1006-7493.2014201 (in Chinese).

Zhao, Y.Y., Zheng, Y.F., 2011. Record and time of Neoproterozoic glaciations on earth. Acta Petrol. Sin. 27, 545–565. https://doi.org/10.14027/j.issn.1000-0550.2019.102 (in Chinese).

Zhao, W.Z., Li, J.Z., Yang, T., Wang, S.F., Huang, J.L., 2016. Geological difference and its significance of marine shale gases in South China. Petrol. Explor. Dev. 43, 499–510. https://doi.org/10.11698/PED.2016.04.01.

Zhao, G.C., Wang, Y.J., Huang, B.C., Dong, Y.P., Li, S.Z., Zhang, G.W., Yu, S., 2018. Geological reconstructions of the east Asian blocks: from the breakup of Rodinia to the assembly of Pangea. Earth-Science Review 186, 262–286. https://doi.org/10.1016/j.earscirev.2018.10.003.

Zhao, K., Li, T.T., Zhu, G.Y., Zhang, Z.Y., Li, J.F., Wang, P.J., Yan, H.H., Chen, Y.J., 2020. Development environment and formation mechanism of lower cambrian source rocks in the chengkou area, Northeast Chongqing, South China. Acta Sedimentological Sinica 38, 1111–1122 (in Chinese).